APPENDIX D. BATHYMETRIC AND HYDRODYNAMIC STUDY

COAST & HARBOR ENGINEERING

Sand Mining Impact Analysis

Supplemental Environmental Impact Report
California State Lands Commission

January 2025

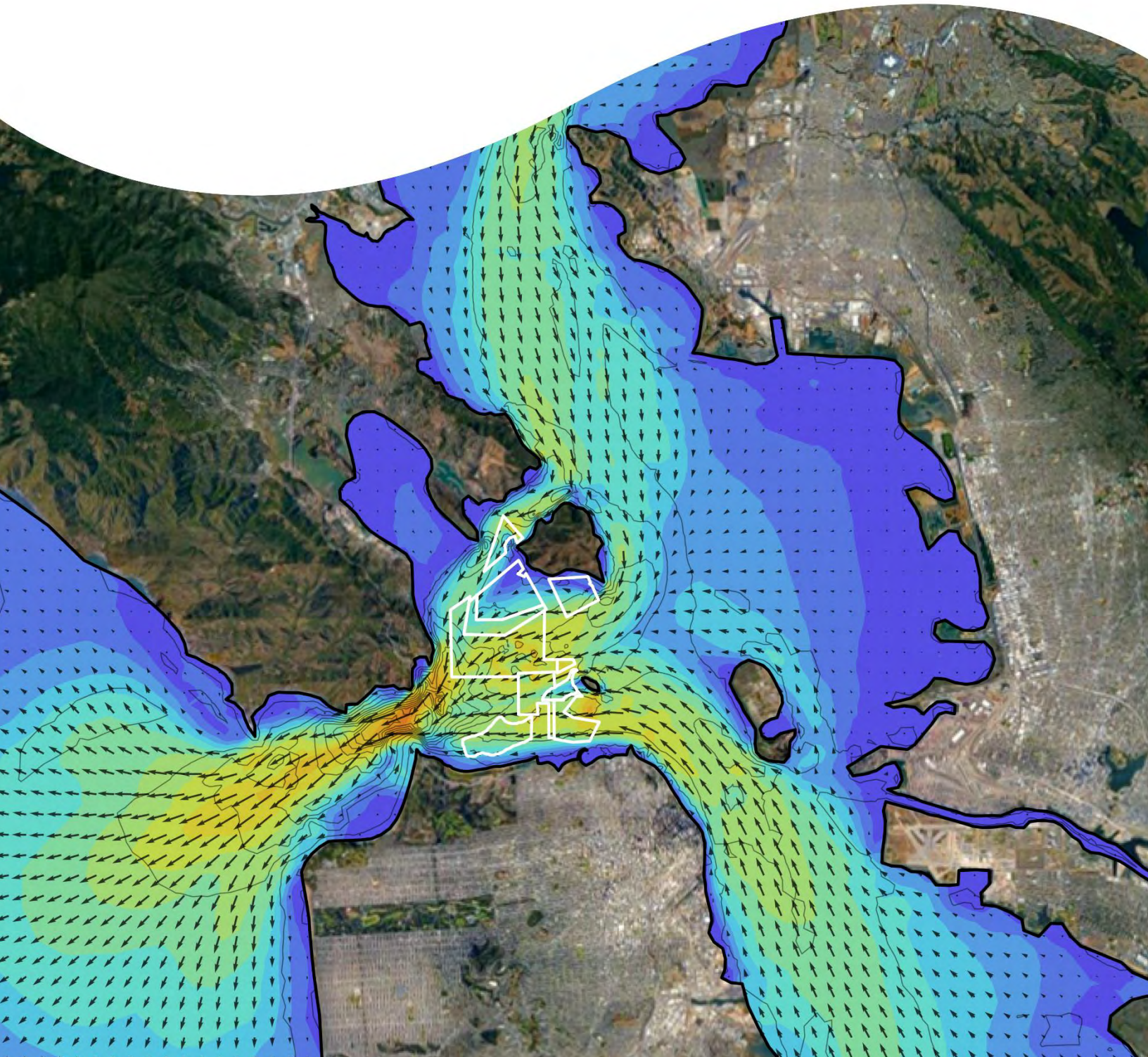

Document Record

Revision	Date	Originator	Checker	Approver	Description
0	November 6, 2024	SF	FS	SF	Initial Draft for Client Review
Final	January 14, 2025	SF	FS	SF	Final

Contents

Tables

Figures

Introduction

Numerical Modeling

Existing Hydrodynamics and Sediment Transport in Lease Areas

Sand Mining Impact Analysis

Sensitivity Tests

Executive Summary

Coast and Harbor Engineering (CHE) performed sediment transport modeling and analysis as a subconsultant to Environmental Science Associates (ESA) under contract to California State Lands Commission (CSLC) to evaluate potential impacts of proposed sand mining in the Central Bay and Suisun Bay areas of San Francisco Bay. The analysis was performed in support of the Sand Mining Supplemental Environmental Impact Report (SEIR), and consisted of numerical modeling of hydrodynamics, sand transport, and bed morphology.

Impacts of *Proposed Mining* were evaluated relative to *No Proposed Mining*. Proposed Mining is defined by the total sand volume proposed to be mined over the next ten years, approximately 17.5 million cubic yards (CY). Proposed Mining was represented in a conservative manner in the numerical modeling: sand volumes equivalent to the entire ten future years of mining were removed from the seabed elevations in the 2019 multibeam hydrographic survey (eTrac 2019) as starting conditions for the one-year simulations.

Numerical modeling results for both Central Bay and Suisun Bay indicate that changes in hydrodynamics, sediment transport, and bed morphology are likely to be confined to the vicinity of the mining areas. The mining areas are predicted to impound sand at greater rates for Proposed Mining than for No Proposed Mining. The sand impounded in the mining areas originates from the immediate surrounding areas, moving more strongly in directions consistent with the local net total transport direction.

Proposed Mining is not likely to cause a significant impact on sediment transport and morphology in areas outside the vicinities of the lease areas, such as the San Francisco Bar or Ocean Beach. Measurable changes in bed elevation caused by the Proposed Mining relative to No Proposed Mining are likely to be limited to the vicinities of the lease areas.

Additional sensitivity testing simulations were performed to evaluate the potential impacts of assumptions and uncertainties on these conclusions. Modeling sensitivity tests included evaluating the effects of excluding full dynamic coupling between hydrodynamics and bed morphology, grain size distribution inputs, and different sand transport formulations. Results of the sensitivity tests confirmed that the conclusions made here are not sensitive to these aspects of the modeling approach and input data.

The analysis also included an assessment of the sand volumes available for mining based on bed elevations in the 2019 multibeam hydrographic survey data (eTrac 2019) and constraints imposed by equipment and permit conditions (see Attachment A).

1 Introduction

1.1 Background

CHE performed coastal engineering analysis as a subconsultant to Environmental Science Associates (ESA) under contract with California State Lands Commission (CSLC) to evaluate potential future sand resources within certain specified CSLC lease areas, and the potential impacts of the Proposed Mining for the next ten years. The study included bathymetry data analysis for the purpose of evaluating sand resources availability, and numerical modeling to determine potential impacts of Proposed Mining on San Francisco Bay hydrodynamics, sand transport, and bed morphology.

1.2 Description of Proposed Sand Mining

Sand mining is proposed within designated CSLC lease areas in Central Bay and Suisun Bay using a variety of dredging methods over the next 10 years. The lease areas in Central Bay and Suisun Bay are shown in Figures 1.1 and 1.2, respectively. Table 1.1 shows the total 10-year Proposed Mining volumes provided by CSLC.

Table 1.1: Proposed 10-Year Mining Volumes[1] by Lease Area

Lease Area	Proposed Mining Volume (CY)
PRC 2036	4,500,000
PRC 709 East	------
PRC 709 North	------
PRC 709 South	2,350,000
PRC 7779 East	------
PRC 7779 North	------
PRC 7779 West	5,500,000
PRC 7780 North	1,600,000
PRC 7780 South	------
PRC 5871	------
Middle Ground	1,200,000
7781 West	------
7781 East	2,350,000
Total	**17,500,000**

1. Ten-year Proposed Mining volumes consist of annual Proposed Mining volumes multiplied by ten.

2 Numerical Modeling

2.1 Initial Bed Change to Represent Mining

To evaluate the potential impacts of Proposed Mining on hydrodynamics, sand transport, and bed morphology, two scenarios were simulated and analyzed: (1) Proposed Mining, and (2) No Proposed Mining. The Proposed Mining scenario consists of the existing bathymetry with Proposed Mining volumes (full 10 years) removed from the mining areas. The No Proposed Mining scenario consists of the existing bathymetry.

Mining is not proposed to occur over entire Lease Areas under the Proposed Mining scenario. Vessel positioning data from 2020-2022 were analyzed and mining locations were relatively consistent. The areas where mining was performed in 2020-2022 were used to delineate the areas to be deepened

for Proposed Mining; however, there were some additional mining areas that were proposed by CSLC. A single mining depth was calculated for each delineated mining area such that the product of this depth and the area equal the total ten-year mining volume.

Proposed Mining impacts were represented in a highly conservative manner in the numerical modeling, because to represent the mining, the entire sand volumes equivalent to ten future years of mining were removed from the seabed elevations in the 2019 multibeam hydrographic survey (eTrac 2019) to serve as starting conditions for the simulations. In reality, mining occurs slowly over time and the changes in hydrodynamics and bed morphology would be very gradual, resulting in significantly smaller initial morphology changes in response to the mining-related deepening.

Figure 2.1 shows the mining zones and depths assumed for Proposed Mining, for Central Bay and Suisun Bay. As noted above, Proposed Mining is assumed to occur in the areas where vessel positioning data showed frequent mining in recent years, with the addition of a slightly larger Proposed Mining area in Suisun Bay Lease Area 7781 East.

As noted above, 2019 multibeam bathymetry data were used in the modeling domain where available for both Proposed Mining and No Proposed Mining scenarios, since the 2019 multibeam was the latest available dataset when this analysis was initiated. eTrac performed a multibeam hydrographic survey in 2023 (eTrac 2023). eTrac reported mean vertical elevation differences of only 0.5 ft (0.15 m) and 0.1 ft (0.04 m) for Central Bay and Suisun Bay, respectively, between the 2019 and 2023 data. Therefore, overall elevation changes between the two surveys were small relative to the total depths in the areas and would not have a significant effect on the analysis. In addition, as discussed in Section 4, impacts to due to mining activities are assessed in this analysis by directly comparing modeling results between Proposed Mining (2019 bathymetry with 10 years of mining volumes removed), and No Proposed Mining (2019 bathymetry). Since the analysis evaluates sand mining impacts through direct comparison (subtraction) of hydrodynamics and sediment transport/morphology between the two modeling scenarios, and changes from 2019 to 2023 are small relative to total water depths, the analysis of impacts from Proposed Mining is not measurably affected by the choice of background bathymetry data (2019 vs. 2023).

2.2 Model Selection

Numerical modeling was performed to evaluate potential impacts of sand mining on hydrodynamics, sediment transport, and bed morphology. A Mike3 Flexible Mesh (Mike3FM) model (DHI 2023a) of the San Francisco Bay estuary was constructed and validated. Mike3FM was used to simulate three-dimensional (3D) hydrodynamics and salinity, and sand transport and bed morphology within the Sand Transport (ST) module (DHI 2023b). Mike3FM was selected for the analysis based on its accurate 3D simulation of hydrodynamics and salinity, and capability to simulate multi-fraction sand transport.

Mike3FM solves 3D incompressible Reynolds-averaged Navier-Stokes shallow water equations, in a conservative form, using a cell-centered finite volume method. Time integration is performed using a semi-implicit scheme. The Sand Transport (ST) module includes a multi-fraction simulation capability that allows spatially variable sand grain size distributions. The model utilizes the sand transport formulation of Wilcock et al (2003) and a multi-layered bed representation allowing vertical bed stratification and armoring.

The primary one-year simulations excluded full dynamic coupling between the hydrodynamics and bed morphology, for conservatism and computational efficiency. In a fully coupled hydrodynamic and morphology model, morphological changes cause continual changes to hydrodynamics, which in turn affect morphological changes. Consequently, in a fully coupled hydrodynamic model, the rate of morphological change will lessen over time as hydrodynamics adapt to the updated morphology (in

this case, deposition in a mining area after dredging). In a decoupled model, hydrodynamic patterns remain the same regardless of morphological changes that occur during the simulation; those hydrodynamics continuously drive the same rate of morphological change. Use of a decoupled model is conservative because impacts on hydrodynamics (and hence bed morphology) do not tend to lessen over time as the mined areas impound sediments. Sensitivity analysis was performed to evaluate the effects of excluding full dynamic coupling between hydrodynamics and morphology, as well as sand grain size input assumptions, and choice of sand transport model formulation (Section 5).

2.3 Model Domain

The model domain (Figure 2.2) includes the San Francisco Bay Estuary, from approximately 42 miles offshore in the Pacific Ocean to the lower reaches of the Sacramento and San Joaquin Rivers. The model domain consists of an unstructured mesh composed of triangles and quadrilaterals with variable resolution, facilitating large variations in resolution and faster computation. The grid includes 24,577 nodes and 34,894 elements with sizes ranging in length from approximately 4.5 miles at the ocean boundary to approximately 250 feet in the lease areas. Higher resolution was used in the lease areas to resolve local bathymetric and hydrodynamic features. Figure 2.3 and Figure 2.4 show close-up views of the model bathymetry (2019 bathymetry) and model grid for Central Bay and Suisun Bay, respectively. A sigma-layer vertical grid system was used with seven equal layers, each a constant percentage of the total depth. Vertical layer thicknesses change over time as total water depths fluctuate. A constant roughness height of 0.017m was prescribed uniformly throughout the domain, which generated bed shear stresses roughly equivalent to those generated using a Manning's roughness of 0.02.

2.4 Boundary Conditions

Boundary conditions included Pacific Ocean tides and Delta outflow. DAYFLOW (California Department of Water Resources 2023) model data were used to represent the Delta outflow. Offshore water level boundary conditions were developed using eight (8) tidal harmonic constituents extracted from the DTU10 global tide model constituent database (Cheng et al 2010). Winds measured at San Francisco were input to the model in all simulations (NOAA Station 9414290, San Francisco). Waves were excluded from the modeling as wave-induced transport effects near the lease areas are anticipated to be minimal (wind-waves over lease areas do not affect bed shear stresses since wave heights are small relative to total depth), and wave effects are similar for both Proposed Mining and No Proposed Mining. No sand load boundary conditions were applied in the rivers.

2.5 Sand Size Inputs

The initial sediment bed in the model was constructed using grain size measurements from Barnard et. al (2013a), McGill et. al (2020), Allen et. al (2021), USGS (2019), and 2022 quarterly mining reports provided by CSLC. Full grain size distributions from each available sample were used to develop a Bay-wide gridded representation of the grain size distributions. Figure 2.5 shows the sample locations and median grain diameters used to develop the Bay-wide sand grain size distribution map. Since the focus of the analysis is sand transport, only sand was simulated. Finer Bay Mud and larger material (e.g., medium gravel) were not included in the simulations (described below).

Eight sand classes were defined, ranging from very fine sand to small gravel according to the Wentworth designation. Sand grain size distributions were modeled using the following eight sand size classes: 0.125, 0.177, 0.250, 0.354, 0.50, 0.707, 1.0, and 2.0 mm. In each model grid cell, each of these size classes was assigned a percentage of the bed based on measured grain size distributions from field samples. In areas with measured median grain size smaller than 0.125 mm, the entire bed was designated to be entirely made up of the finest fraction (gradation with 0.125 mm median diameter). In

areas with measured median grain sizes larger than 2.0 mm, the entire bed was designated to be entirely made up of the largest fraction (gradation with 2.0 mm median diameter). The grain size distributions in the areas to be mined were uniform and were defined using the average measured grain sizes reported by the mining companies in the four quarterly reports from 2022. The gradations representing each mining area were developed by averaging the fractions of sand within each size range from each mining quarterly report.

2.6 Hydrodynamic Model Validation

Simulated water levels and current velocities were validated using NOAA predicted tides and current velocities measured at the locations shown in Figure 2.6. Figure 2.7 shows comparisons of predicted and simulated water levels at the NOAA stations. The water level validation is excellent in the offshore and Central Bay areas and reasonable at locations near Suisun Bay. The numerical model was also validated using Acoustic Doppler Current Profiler (ADCP) measurements taken at three different locations during NOAA field data collection campaigns, including Bay Bridge Pier D, Davis Point, and Carquinez Strait. Current velocities at these three locations were compared at multiple locations from near-bottom measurement bins to near-surface measurement bins.

Figure 2.8 and Figure 2.9 show comparisons between measured and predicted velocities at Davis Point and Carquinez Strait, respectively (current survey by NOAA in 2013). Davis Point velocities reach 2-3 ft/s while Carquinez Strait velocities reach 4-6 ft/s, depending on measurement depth. The numerical model predictions closely match the measured velocities at all depths, and at both locations.

Figure 2.10 shows a comparison between measured and predicted velocities at Bay Bridge Pier D (current survey by NOAA in 2012) at different depths from near-bottom measurement bins to near-surface measurement bins. Current velocities reach 4-6 ft/s at this location depending on measurement depth. As in the other locations, the numerical model predictions closely match the measured velocities at all depths. Overall, the validation results demonstrate that the hydrodynamic model accurately captures the hydrodynamics of the Bay in locations both north and south of Central Bay.

2.7 Simulation Periods

Two separate one-year time periods were simulated to capture a range of Delta outflow conditions: a low-flow period, and a high-flow period. Figure 2.11 shows the total Delta outflow from the DAYFLOW model from 2008 to 2020, the selected simulation periods, and the model validation periods. The low-flow period was selected to be from June 15, 2014, to June 15, 2015. The high-flow period was selected to be from June 15, 2018, to June 15, 2019. Given that the analysis is intended to represent long-term potential impacts of the Proposed Mining relative to No Proposed Mining, extreme conditions (i.e., driest, or wettest years) were not simulated.

3 Existing Hydrodynamics and Sediment Transport in Lease Areas

3.1 Central Bay

Figure 3.1 shows instantaneous snapshots of typical near-bottom peak ebb (left) and flood (right) currents in Central Bay for existing conditions, during the low-flow period. Peak near-bottom current velocities during a typical spring tide vary considerably within the lease areas and reach up to 5-6 feet per second.

Sand transport was simulated for both the low-flow and high-flow time periods discussed in Section 2.7. Model results include total sand transport and bed morphology. Maps of one-year net total sand transport were calculated for existing conditions to demonstrate existing transport patterns predicted by the multi-fraction sand transport model. Net transport was calculated by summing vector components of sand transport rates at each model output time step throughout the simulation duration. Figure 3.2 shows vectors depicting the directions of net total sand transport in Central Bay, with vector length and color depicting magnitude, for the low-flow simulation (left) and high-flow simulation (right).

The patterns are similar in most areas regardless of Delta outflow because Central Bay is tidally dominated. In northern Central Bay, flood-directed net total transport dominates in the lease areas. In southern Central Bay, ebb-directed net total transport dominates in the lease areas. In the high-flow year, flood-directed net total sand transport in northern Central Bay is slightly weaker. In the high-flow year, ebb-dominated net total sand transport is similar in southern Central Bay, and flood-dominated net total sand transport is stronger just outside the Golden Gate.

Figure 3.3 shows the predicted net total sand transport as a percentage of the gross total sand transport (net total transport vectors for No Proposed Mining). Results in Central Bay indicate that net total transport can range from a low percentage of gross total transport (5-10%), to a majority of gross total transport (greater than 80%), depending on location. This spatial variability in net total transport is logical given the highly variable hydrodynamic and sand transport patterns in Central Bay.

A qualitative validation of sand transport direction was performed by comparing modeled net transport directions with net transport directions inferred from bedform asymmetry observations (Barnard et al. 2013b). Figure 3.4 (left) shows the one-year net total sand transport vectors colored either to represent either ebb (red) or flood (blue) transport directions, for low-flow conditions. Figure 3.4 (right) shows net sand transport direction inferred from bedforms as reported by Barnard et al. (2013b). The predicted patterns of net total transport direction (ebb vs. flood) visually compare well with the measured bedform asymmetry in most areas including the areas proposed for mining, indicating that the model results reasonably represent both the hydrodynamics and net sand transport in Central Bay over relatively long time periods.

3.2 Suisun Bay

Figure 3.5 shows snapshots of typical peak ebb (left) and flood (right) near-bottom currents under existing conditions in Suisun Bay. Higher velocities are concentrated in narrower channel areas and reach up to approximately 3 feet per second. The Middle Ground lease area experiences lower velocities than 7781 East due because Middle Ground is situated in a wider overall channel.

Figure 3.6 shows vectors depicting the directions of net total sand transport, with vector length and color depicting magnitude, for the low-flow simulation (left) and high-flow simulation (right). Results from the low-flow simulation indicate mixed directions of net total transport (flood-directed, and ebb-directed) in the deeper channel areas, with stronger ebb-directed net total transport on the north side of lease area 7781 East, and flood-directed net total transport south of lease area 7781 East. During the high-flow year when river discharge adds to ebb flows, most of the area experiences ebb-directed net total transport, except for the area south of lease area 7781 East.

Figure 3.7 shows the predicted net total sand transport as a percentage of the gross total sand transport, and net total transport vectors for No Proposed Mining. Results in Suisun Bay indicate that net total transport (as a percentage of gross) also strongly varies, similar to Central Bay. Shallower areas tend to have a net total sand transport that is a larger portion of the gross total sand transport. The mining zones within the lease areas have net total sand transport magnitudes that are a greater

percentage of gross total sand transport during the high-flow simulation than the low-flow simulation, when river discharge causes additional ebb-directed transport.

A qualitative sand transport validation was also performed for Suisun Bay, by comparing net sand transport patterns with net transport patterns inferred from bedform asymmetry (Barnard et al. 2013b). Figure 3.8 (left) shows one-year net total sand transport vectors colored to represent either ebb (red) or flood (blue) transport directions, during low-flow conditions. Figure 3.8 (right) show net sand transport direction inferred from bedforms (Barnard et al. 2013b). The predicted patterns of net total transport direction (ebb vs. flood) compare well with the measured bedform asymmetry in most areas including Middle Ground and lease area 7781 East, indicating that the model results reasonably represent both the hydrodynamics and net sand transport in Suisun Bay over relatively long time periods.

4 Sand Mining Impact Analysis

4.1 Impacts to Central Bay Hydrodynamics

Figure 4.1 shows differences in near-bottom current speeds caused by Proposed Mining relative to No Proposed Mining at peak ebb (left) and flood (right), during low-flow conditions. Differences in current speeds were computed at a single instantaneous snapshot (model time step), which is a conservative way to calculate changes because the introduction of bathymetry changes can cause small shifts in the timing of peak velocities. Small changes in timing can produce changes in an instantaneous map that may not be significant when measuring time histories of current speed at a specific location.

Analysis indicates that near-bottom current velocity patterns surrounding the lease areas are similar between Proposed Mining and No Proposed Mining during peak ebb and flood currents. Changes in near-bottom current speeds are less than approximately 0.3 feet/sec (10-15%) over most of the mined areas and reach a maximum of 0.8 feet/sec in Lease Area 7780. Near-bottom velocity changes are generally less than 0.1 feet per second in areas outside the vicinities of the lease areas. It should be noted that the elevations of the near-bottom cells are different for Proposed Mining and No Proposed Mining since both models utilize a pure sigma-layer vertical grid.

4.2 Impacts to Central Bay Sediment Transport and Bed Morphology

Figure 4.2 shows differences in net total sand transport caused by Proposed Mining relative to No Proposed Mining, for the low-flow simulation (left), and high-flow simulation (right). Results indicate that net total sand transport patterns are affected most in the deepened lease areas, and to a lesser degree in the general vicinities (within roughly 1,000 feet) of the lease areas. Patterns of net total sand transport changes are similar to patterns of hydrodynamic changes caused by Proposed Mining relative to No Proposed Mining.

Figure 4.3 shows one-year bed changes (erosion and accretion) caused by Proposed Mining relative to No Proposed Mining, for the low-flow simulation (left), and high-flow simulation (right). Results indicate that bed change differences caused by Proposed Mining relative to No Proposed Mining are greater than 1.5 feet only within and near the edges of the mined areas, and less than 0.3 feet outside the vicinity of the lease areas. Relative bed changes predicted in the modeling are consistent with where the areas were deepened, and the extent to which they were deepened for Proposed Mining. The deposited sand was eroded from the edges of the mined areas, which is characteristic of sand near-bed transport surrounding a deepened area. In general, Proposed Mining results in greater deposition in mined areas and increases in erosion immediately upstream and downstream of the

mined areas. The largest deposition for Proposed Mining relative to No Proposed Mining occurs in Lease Area 7780, because the Proposed Mining depth is largest, and Lease Area 7780 is erosional under No Proposed Mining conditions. The relative bed change was computed by subtracting an erosion rate from a larger deposition rate, resulting in a large *relative* bed change for Proposed Mining.

Figure 4.4 shows volumetric trends of erosion and deposition in the mined areas of Central Bay, along with total Delta outflow. The deepened portions of all four Central Bay lease areas show depositional trends for Proposed Mining, and all but Lease Area 7780 (as discussed above) show depositional trends for No Proposed Mining. Results indicate that Lease Area 7780 is erosional under No Proposed Mining. Lease Area 7780 becomes depositional for Proposed Mining because of the larger increase in depth after mining. In all lease areas, deposition is larger for Proposed Mining than for No Proposed Mining.

Volumetric changes over time indicate that Delta outflow influences deposition and/or erosion in the mined areas, but the trends vary by lease area depending on its location in Central Bay. Deposition and erosion trends are largely linear during the low-flow simulation but are affected by Delta outflow during the latter half of the high-flow simulation. Among all Central Bay lease areas to be mined, volumetric change trends in the deepened portion of Lease Area 709 are least affected by Delta outflow. Lease areas 2036 and 7780 show higher deposition rates during the high-flow simulation than the low-flow simulation, due to reduced net total sand transport through the deepened areas during high flows (see net total transport in Figure 3.2). Lease areas 709 and 7779 show similar deposition rates during the low-flow and high-flow simulations, albeit slightly higher during the low-flow simulation.

4.3 Impacts to Suisun Bay Hydrodynamics

Figure 4.5 shows changes in peak near-bottom current speeds caused by Proposed Mining relative to No Proposed Mining during peak ebb (left) and peak flood (right) currents in Suisun Bay, during low-flow conditions. In comparison to Lease 7781, Middle Ground shows Proposed Mining causing a larger reduction in current speeds relative to No Proposed Mining, due to larger Proposed Mining depth/volume over a smaller area. Small increases in near-bottom velocity (approximately 0.2 feet per second) are predicted downstream of the deepened area at Middle Ground, likely in response to a shift in velocity patterns that becomes visible when directly subtracting instantaneous velocity snapshots.

Overall, during peak flood currents, reductions in near-bottom velocities are lower than changes observed during peak ebb currents. Changes are anticipated to be less than 0.2 feet per second over the majority of the lease areas, except for a portion of the mined area at Middle Ground which experiences a decrease in current speed of up to 0.5 feet per second during peak ebb currents.

4.4 Impacts to Suisun Bay Sediment Transport and Bed Morphology

Figure 4.6 shows changes in net total transport caused by Proposed Mining relative to No Proposed Mining, for the low-flow simulation (left), and high-flow simulation (right). Results indicate that net total sand transport patterns are primarily affected in the vicinities of the lease areas. At Middle Ground, changes are observed slightly upstream and downstream, and to the south due to some redistribution of flows south of Middle Ground. At 7781 East, changes in net total transport are anticipated to be largely limited to within the lease area.

Figure 4.7 shows the differences in one-year bed change caused by Proposed Mining relative to No Proposed Mining, for the low-flow simulation (left), and high-flow simulation (right). Relative bed changes are greater for the high-flow simulation than the low-flow simulation, due to the influence of Delta outflow in Suisun Bay. Bed change differences caused by Proposed Mining relative to No Proposed Mining are

greater than 0.3 feet in areas within the mined areas and adjacent to the lease areas, and less than 0.3 feet outside the vicinities of the lease areas.

Predicted relative bed changes are logical based on the locations of mined areas and differences in depths for Proposed Mining relative to No Proposed Mining. The deepened area at Middle Ground under Proposed Mining impounds more sediment than the same area for No Proposed Mining. Sand is eroded from the edges of the deepened areas, which is logical for near-bed sand transport; however, in Suisun Bay, the influence of Delta outflow is stronger which makes the erosion patterns around the deepened areas less symmetrical than in Central Bay.

Figure 4.8 shows volumetric trends of erosion and deposition in the mined areas, along with total Delta outflow. Volumetric changes over time indicate that Delta outflow has a stronger influence on deposition/erosion trends in the deepened areas at Middle Ground than at 7781 East. At Middle Ground, deposition and erosion trends are largely linear during the low-flow simulation but are affected by Delta outflow during the latter half of the high-flow simulation. High Delta outflows change this portion of Middle Ground from depositional to erosional. The deepened portions of both Suisun Bay lease areas show depositional trends for Proposed Mining, during the entirety of the low-flow and high-flow simulations.

Under No Proposed Mining, results indicate that the deepened portion of Middle Ground (Lease Area 39) is erosional during high-flow conditions. This is logical given that net total transport through the deepened area of Middle Ground is stronger during high flows (see net total sand transport in Figure 3.6). Volumetric change trends in the deepened portion of 7781 East are largely linear for Proposed Mining.

4.5 Impacts to Bed Morphology at the San Francisco Bar

Changes in bed elevation caused by Proposed Mining relative to No Proposed Mining were used to evaluate the effect of Proposed Mining on sand supply to the San Francisco Bar. Bed elevation changes at the Bar caused by Proposed Mining relative to No Proposed Mining would not be measurable (less than one millimeter). However, these small elevation changes were summed over the San Francisco Bar within the polygons shown in Figure 4.9, which includes areas above approximate elevation -45 feet (MLLW). Volumetric changes were computed at the end of the one-year low-flow and high-flow simulations. Results show that Proposed Mining relative to No Proposed Mining causes a net deficit of sand over this area of approximately 3,800 CY following the one-year low-flow simulation period, and approximately 2,800 CY following the one-year high-flow simulation period. These sand volumes are negligible over the large area of the San Francisco Bar. These sand deficits are conservative due to the assumption that the entire 10-year Proposed Mining volumes were extracted prior to the initiation of the simulations.

5 Sensitivity Analysis

Sensitivity analysis was performed using the 3D hydrodynamic model and sand transport model to evaluate the influence of assumptions and input data on the impact analysis conclusions. Simulations were performed to evaluate the effect of excluding full dynamic coupling between hydrodynamics and bed change (excluded for conservatism and computational efficiency), potential uncertainty in the assumed sediment grain size distributions, and uncertainties posed by selection of sand transport formulation.

5.1 Full Dynamic Coupling of Hydrodynamics and Bed Change

The base simulations used for impact analysis did not include full dynamic coupling of predicted hydrodynamics and bed change, i.e., continually updating bed elevation and feedback on hydrodynamics. In the “decoupled” simulations, the hydrodynamic predictions were made using the bed elevations representing the removal of ten years’ worth of mining at the start of the simulation for the entire model run. Bed changes that are predicted to occur during the model run do not affect the hydrodynamics. This “decoupled” approach was used for conservatism and computation speed. In simulations where hydrodynamics and bed change are fully dynamically coupled, the impacts of the deepened mining areas on transport would lessen over time as the deepened areas impound sediment and this changing bed in turn changes hydrodynamics during the simulation. To evaluate the effects of excluding full dynamic coupling, a 4-month sensitivity test simulation was performed using the decoupled approach (base simulation) and the full dynamic coupling approach.

Figure 5.1 shows the 4-month Central Bay bed changes caused by Proposed Mining relative to No Proposed Mining for the decoupled approach (base simulation, left), and full dynamic coupling approach (right), during the low-flow simulation. Figure 5.2 shows the same results for Suisun Bay. For both Central Bay and Suisun Bay, results show that the erosion and deposition caused by Proposed Mining relative to No Proposed Mining for the decoupled (base) simulation is very consistent with, but slightly larger in magnitude than, the fully coupled simulation.

Since depths are relatively large in Central Bay, differences between the full dynamic coupling and decoupled approaches are minimal during the 4-month simulation. However, in Suisun Bay, where depths are shallower, the use of full dynamic coupling results in a less conservative evaluation of Proposed Mining impacts relative to No Proposed Mining. Over a full one-year period, the difference in results between these two simulation approaches is anticipated to grow, making the decoupled (base) simulation approach more conservative. The sensitivity test showed that the approach of using decoupled hydrodynamics and bed change is conservative for evaluating impacts of Proposed Mining relative to No Proposed Mining.

5.2 Grain Size Assumptions

The sand transport modeling was performed using eight (8) different grain sizes that were used to develop grain size distributions in each cell of the model grid. However, uncertainties exist in the spatial distribution of sand grain sizes because grain size data are relatively sparse. Therefore, a one-year (high-flow) sensitivity test simulation was performed to evaluate the effects on impact analysis conclusions made using results from the base simulation (variable grain sizes), assuming a different sand size distribution. The additional senstivity test simulation was performed using the same Wilcock et al (2003) multi-fraction sand transport formulation, but assuming sand with a constant median grain size of 0.25 mm was present throughout the entire domain. Results were directly compared with the results of the one-year high-flow simulation using variable grain sizes.

Figure 5.3 shows the difference in one-year bed change caused by Proposed Mining relative to No Proposed Mining in Central Bay, for the variable grain size distribution (base simulation, left), and for uniform median grain size of 0.25 mm (right), during the high-flow simulation. As anticipated, bed changes caused by Proposed Mining relative to No Proposed Mining are larger (and over-predicted) when assuming a uniform bed of finer sand than has been measured in many areas of Central Bay. However, the changes occur in generally the same areas, with similar patterns.

Figure 5.4 shows the difference in one-year bed change caused by Proposed Mining relative to No Proposed Mining in Suisun Bay, for the variable grain size distribution (base simulation, left), and for uniform median grain size of 0.25 mm (right), during the high-flow simulation. Differences between bed change impacts for constant 0.25 mm sand and variable grain size sand are not as pronounced

in Suisun Bay as in Central Bay due to smaller sand in the vicinity of the lease areas in Suisun Bay. The sensitivity test showed that the locations of deposition and erosion caused by Proposed Mining relative to No Proposed Mining shown in the impact analysis are valid even if sand grain sizes are smaller and less spatially variable.

5.3 Sand Transport Formulation

A sensitivity test was also performed to evaluate the potential influence on conclusions made here from the choice of sand transport formulation. A one-year high-flow simulation using the van Rijn sand transport formulation (van Rijn 1984) was performed and results were compared with the Wilcock et al (2003) formulation used for the base simulations. As with many other sand transport formulations, van Rijn (1984) does not consider variable grain size distributions. Therefore, for the purposes of the transport formulation sensitivity test, a constant median grain size of 0.25 mm was used throughout the domain for both simulations, and results using the van Rijn (1984) formulation were compared directly with results using the multi-fraction transport Wilcock et al (2003) formulation with constant median grain size of 0.25 mm.

Figure 5.5 and Figure 5.6 show the bed changes caused by Proposed Mining relative to No Proposed Mining when using the multi-fraction Wilcock et al (2003) formulation with constant median grain size 0.25 mm (left), and van Rijn (1984) formulation with constant median grain size 0.25 mm (right), for Central Bay and Suisun Bay, respectively (one-year high-flow simulation). *Note that the results shown in Figures 5.5 and 5.6 do not include the base simulation results used as the basis for conclusions regarding sand mining impacts.*

For both Central Bay and Suisun Bay, the results show that the changes in erosion and deposition caused by Proposed Mining relative to No Proposed Mining occur in the same areas, with very similar patterns, regardless of the sediment transport formulation selected. The magnitudes of relative erosion and deposition are larger for tests with uniform 0.25 mm grain size (as discussed in the previous section), and slightly greater in some areas when using the van Rijn (1984) formulation as compared to the Wilcock et al (2003) formulation. However, the patterns and magnitudes of erosion and deposition caused by Proposed Mining relative to No Proposed Mining are consistent regardless of sand transport model formulation used in the simulations.

6 Conclusions

Impacts of sand mining were analyzed using conservative assumptions in a numerical modeling evaluation: the entire ten years of mining was assumed to occur prior to the beginning of the simulations, which in the numerical modeling caused significantly larger changes in hydrodynamics and transport than would occur under gradual mining. This approach is expected to show an upper bound on the impacts of sand mining in these areas. In addition, full dynamic coupling between hydrodynamics and bed change was excluded in the modeling, which prolongs the stronger hydrodynamic changes in the modeling that are generated immediately following the deepening of the seabed (ten-year volume all at once).

Analysis of the conservative numerical modeling results indicates that relative to No Proposed Mining, the Proposed Mining is not likely to cause a significant impact on sediment transport and sand budgets in areas outside the vicinity of the lease areas, such as the San Francisco Bar or Ocean Beach. Changes in bed elevation caused by the Proposed Mining relative to No Proposed Mining are likely to be limited to the vicinities of the lease areas.

7 References

Allen, R.M., Lacy, J.R., McGill, S.C., and Ferreira, J.C.T., 2021. *Hydrodynamic, Sediment Transport, and Sediment Flocculation Data from South San Francisco Bay, California, Summer 2020*: U.S. Geological Survey data release, https://doi.org/10.5066/P99Q4CHM.

Barnard, P.L., Foxgrover, A.C, Elias, E., Erikson, L., Hein, J.R., McGann, M.L., Mizell, K., Rosenbauer, R.J; Swarzenski, P.W., Takesue, R.K., Wong, F.L., Woodrow, D.L. 2013a. *Grain Size Analyses of Sediment Samples from the San Francisco Bay Coastal System*. https://doi.org/10.1594/PANGAEA.804477.

Barnard, P.L., Foxgrover, C; Elias, Edwin; Erikson, Li H; Hein, James R; McGann, Mary L; Mizell, Kira; Rosenbauer, Robert J; Swarzenski, Peter W; Takesue, Renee K; Wong, Florence L; Woodrow, D.L. 2013: *San Francisco Coastal System grain size and geochemical data for sand provenance study*. https://doi.org/10.1594/PANGAEA.803904.

Barnard, P.L., L.H. Erikson, E.P.L. Elias, and P. Dartnell. 2013b. *Sediment Transport Patterns in the San Francisco Bay Coastal System from Cross-Validation of Bedform Asymmetry and Modeled Residual Flux*. Marine Geology 345:72-95.

California Department of Water Resources. 2023. *DAYFLOW Results 1997-2020.* https://data.cnra.ca.gov/dataset/dayflow. Accessed 3/1/2023

Cheng, Y., Andersen, O.B. 2010. *Improvement in Global Ocean Tide Model in Shallow Water Regions*. Poster, SV.1-68 45, OSTST, Lisbon, Oct.18-22.

DHI. 2023a. *MIKE 3 Flow Model FM Hydrodynamic and Transport Module Scientific Documentation.* https://manuals.mikepoweredbydhi.help/latest/Coast_and_Sea/MIKE_3_Flow_FM_Scientific_Doc.pdf

DHI. 2023b. *MIKE 21 & 3 Flow Model FM Sand Transport Module Scientific Documentation.* https://manuals.mikepoweredbydhi.help/latest/Coast_and_Sea/MIKE_FM_ST_Scientific_Doc.pdf

eTrac. 2019. *Multibeam Hydrographic Survey of Central and Suisun Bays.*

eTrac. 2023. *Central San Francisco Bay and Suisun Bay Sandmining Lease Area Surveys Change Analysis Report April 2023*.

Engelund, F. and Fredsoe, J. 1976. *A Sediment Transport Model for Straight Alluvial Channels*. Nordic Hydrology, 7, pp. 296-306.

McGill, Samantha C., WinklerPrins, L. and Tan, A.C., 2020. *Grain Size, Bulk Density, and Organic Carbon of Sediment Cores from San Pablo Bay and Grizzly Bay, California*. Data Release doi:10.5066/P9P7I65U, U.S. Geological Survey, Pacific Coastal and Marine Science Center, Santa Cruz, California.

NOAA. 2012. *ADCP Current Survey ID SFB1207.* https://tidesandcurrents.noaa.gov/cdata/StationList?type=Current+Data&filter=historic. Accessed November 2022.

NOAA. 2013. *ADCP Current Survey ID SFB1316 and SFB1319*. https://tidesandcurrents.noaa.gov/cdata/StationList?type=Current+Data&filter=historic. Accessed November 2022.

NOAA 2023. *Meteorological Data ID 9414290.* https://tidesandcurrents.noaa.gov/waterlevels.html?id=9414290. Accessed November 2022.

NOAA 2023. *Water Level Data ID 9415020, 9414290, 9414863, 9415102, and 9415144.* https://tidesandcurrents.noaa.gov/waterlevels.html?id=9414290. Accessed November 2022.

van Rijn, L.C. 1984. *Part I: Bed Load Transport*, J. Hyd. Eng., 110, October, and *Part II: Suspended Load Transport*", J. Hyd. Eng., 110, November.

Wilcock, P. R., & Crowe, J. C. 2003. *Surface-based Transport Model for Mixed-Size Sediment*. Journal of Hydraulic Engineering, 129(2), 120-128.

USGS (United States Geological Survey). 2019. *Sediment Grain-Size Data from Vibracore Samples Collected Offshore San Francisco, California, During Field Activity 2019-649-FA from 2019-10-11 to 2019-10-18.*

Attachments

A. Sand Resource Availability Analysis

Volumes of material available for mining were computed using the 2019 multibeam hydrographic survey (eTrac) and constraints imposed by equipment and permit conditions that were provided by CSLC. The survey data were interpolated to the lease areas, and areas subject to these constraints were excluded. Constraints used to define zones where mining is feasible within the lease areas are shown in Table 7.1. The zones delineated based on these constraints are not the same as the areas assumed to be mined in the analysis of sand mining impacts (Section 4). Volumes of material available for mining, subject to the constraints in Table 7.1, are shown in Table 7.2. Volumes in Suisun Bay were computed using the more restrictive constraints for seasonal permit conditions. In the cases of PRC 7779 West and PRC 7780 North, the Proposed Mining volumes exceed the material volumes available under the assumed constraints.

Table 7.1: Criteria Used to Define Zones Feasible for Mining Inside Lease Areas

Location	Constraint	Source of Constraint
Central Bay	Above elevation -90 feet MLLW only	Equipment
	Keep distance 250 feet from any water having a depth of 30 feet (MLLW)	Permit Conditions
	Exclude areas within 100-foot buffer of hard bottom areas in / adjacent to Central Bay mining leases.	Permit Conditions
Suisun Bay	Above elevation -90 feet (MLLW) only	Equipment
	Below elevation -15 feet (MLLW) only	Permit Conditions. Between December 1 and June 30, the restriction is -25 feet.
	Exclude areas within 250 feet of any water having a depth of 9 feet (MLLW).	Permit Conditions

Table 7.2: Approximate Volumes of Material Available in Zones Feasible for Mining

Lease Area	Approximate Volume Available for Mining (CY)	Proposed Mining Volume (CY)
PRC 2036	5,392,500	4,500,000
PRC 709 East	3,819,800	------
PRC 709 North	21,900,600	------
PRC 709 South	12,755,200	2,350,000
PRC 7779 East	7,297,500	------
PRC 7779 North	2,574,700	------
PRC 7779 West	5,272,300	5,500,000
PRC 7780 North	537,000	1,600,000
PRC 7780 South	7,567,700	------
PRC 5871	6,706,900	------
Middle Ground	3,948,700	1,200,000
7781 Lease Area West	5,471,600	------
7781 Lease Area East	59,522,600	2,350,000

Considering the equipment and permit limitations assumed in the analysis, available mining volumes in two of the mining zones within the lease areas are exceeded by the proposed ten-year mining volumes. No replenishment of sand inside the mined areas over time was included in the analysis.

Figures

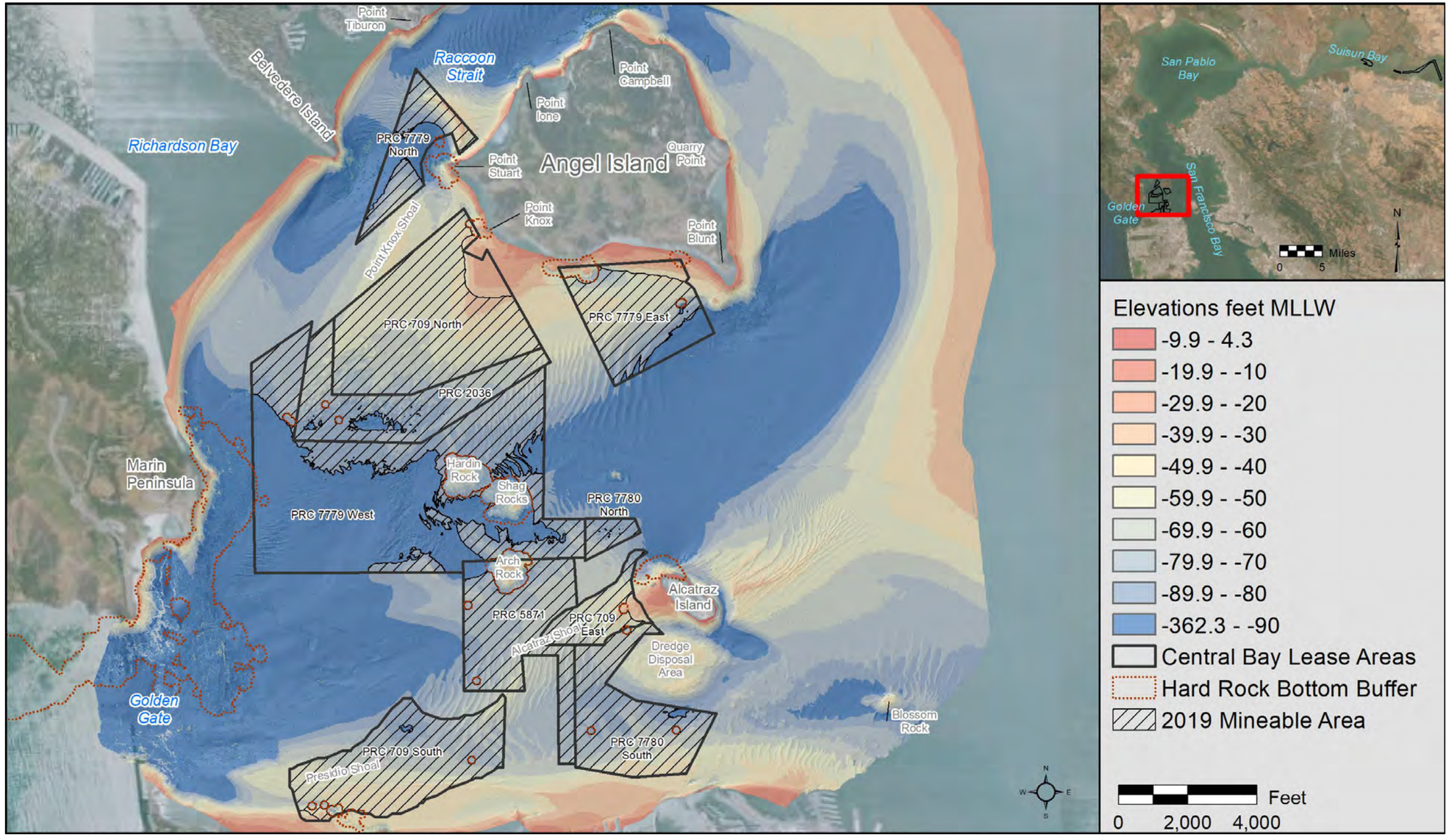

Notes:

1. Hatched areas represent areas where mining is feasible based on reported equipment limitations and where mining is allowed under present permit conditions.

Figure 1.1:

Central Bay Sand Mining Lease Areas

COAST & HARBOR ENGINEERING

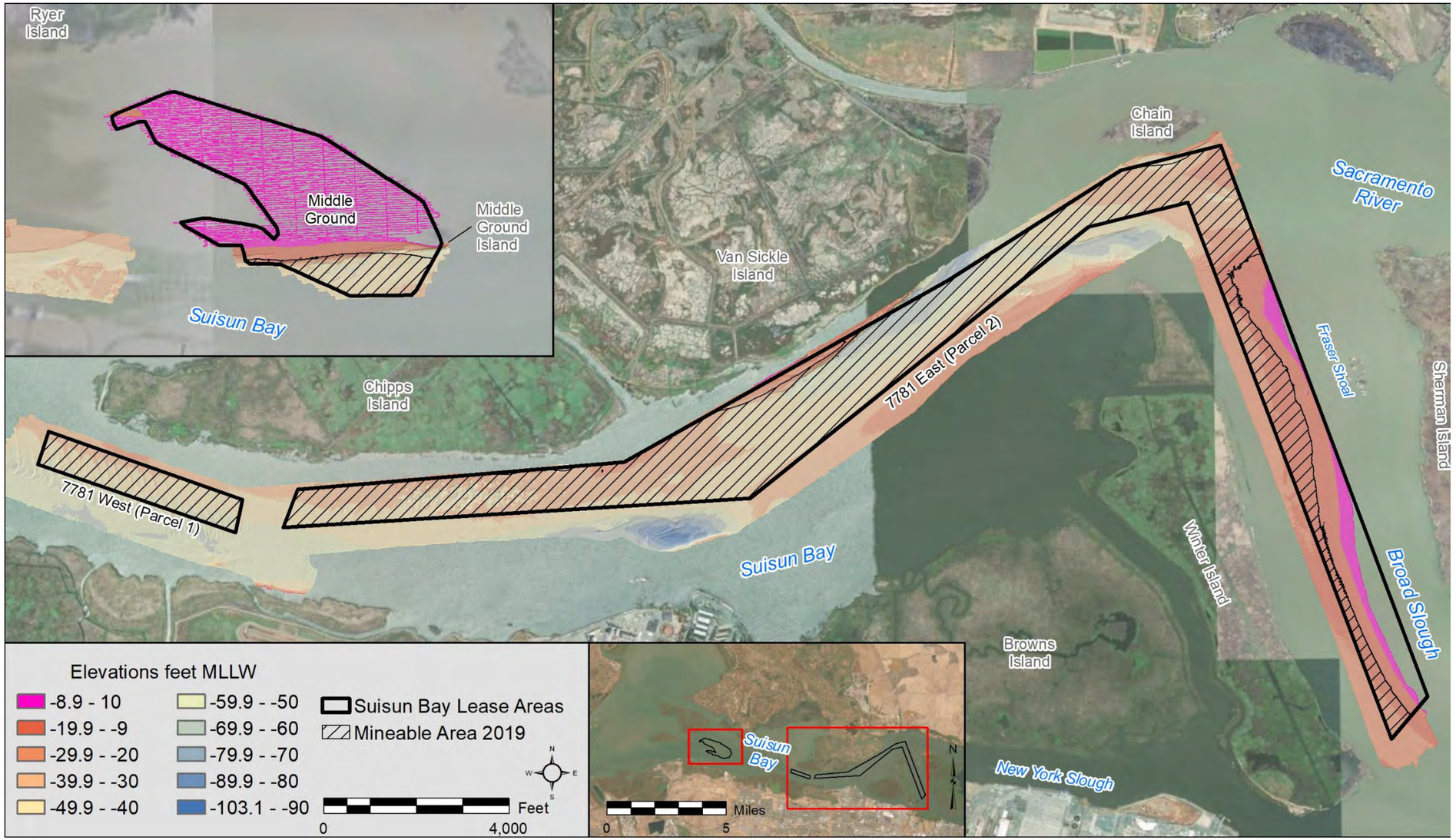

Notes:

1. Hatched areas represent areas where mining is feasible based on reported equipment limitations and where mining is allowed under present permit conditions.

Figure 1.2:

Suisun Bay Sand Mining Lease Areas

COAST & HARBOR ENGINEERING

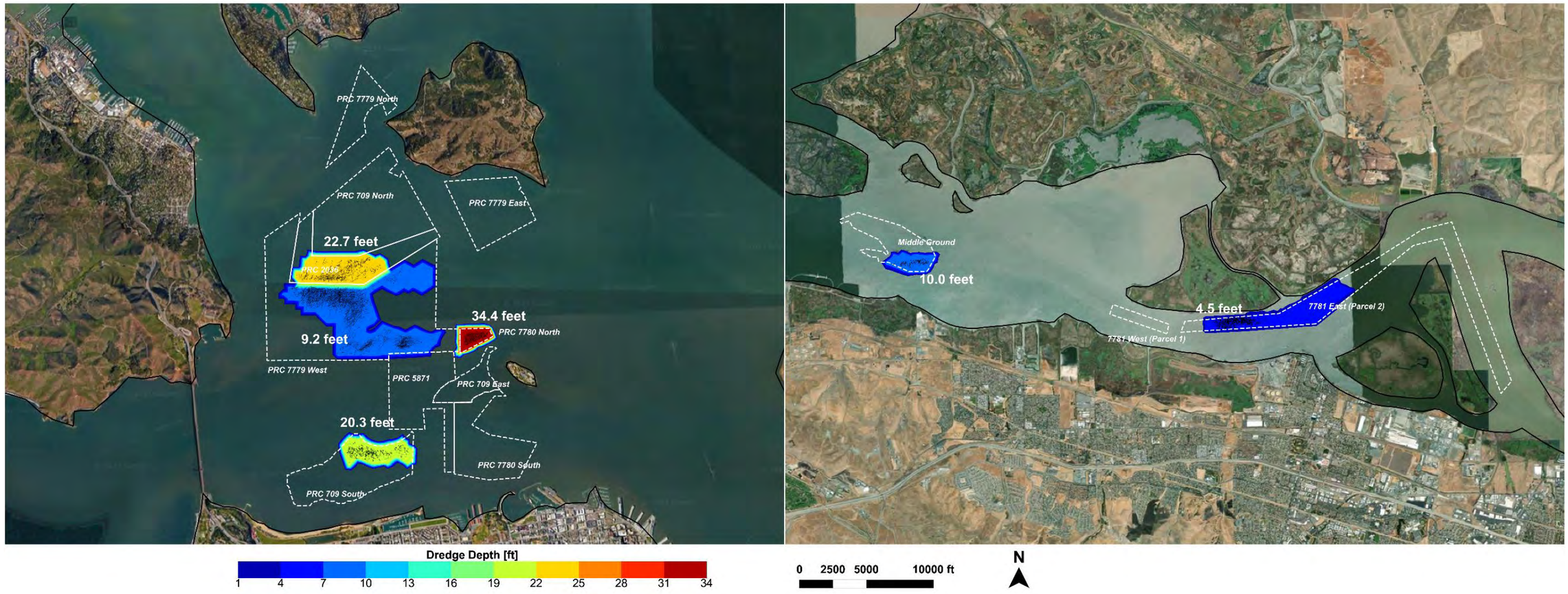

Notes:

1. Black lines represent vessel positioning data from 2020-2022.
2. Mining depths are constant within the areas shown, with depths noted.
3. In Central Bay, mining was assumed to occur in the same areas based on positioning data from 2020-2022 (black lines)
4. At Middle Ground in Suisun Bay, mining was assumed to occur in the same areas based on positioning data from 2020-2022 (black lines)
5. At Lease Area 7781 East in Suisun Bay, Mining was assumed to occur over different areas compared to positioning data from 2020-2022 (black lines)

Figure 2.1:

Proposed 10-Year Mining Depths for Central Bay (Left) and Suisun Bay (Right) 10-Year Mining Depths

COAST & HARBOR ENGINEERING

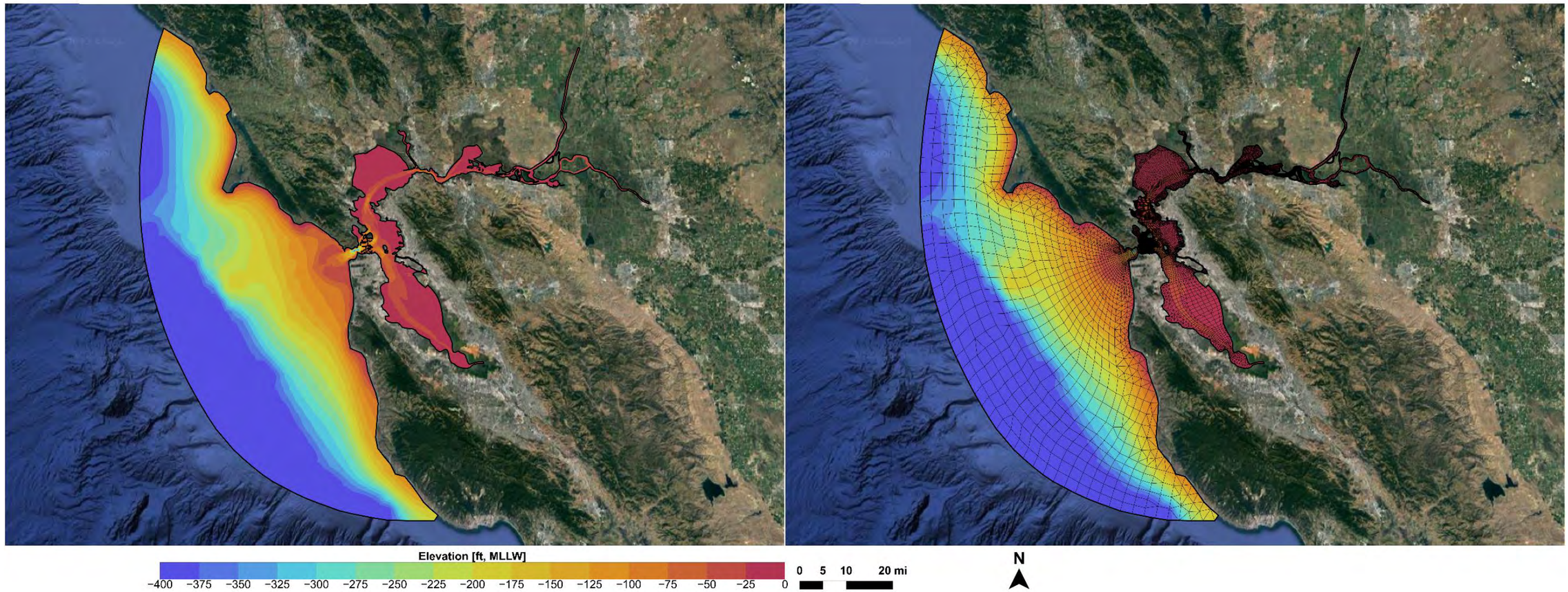

Figure 2.2:

Model Domain Extents (Left) and Grid (Right)

COAST & HARBOR ENGINEERING

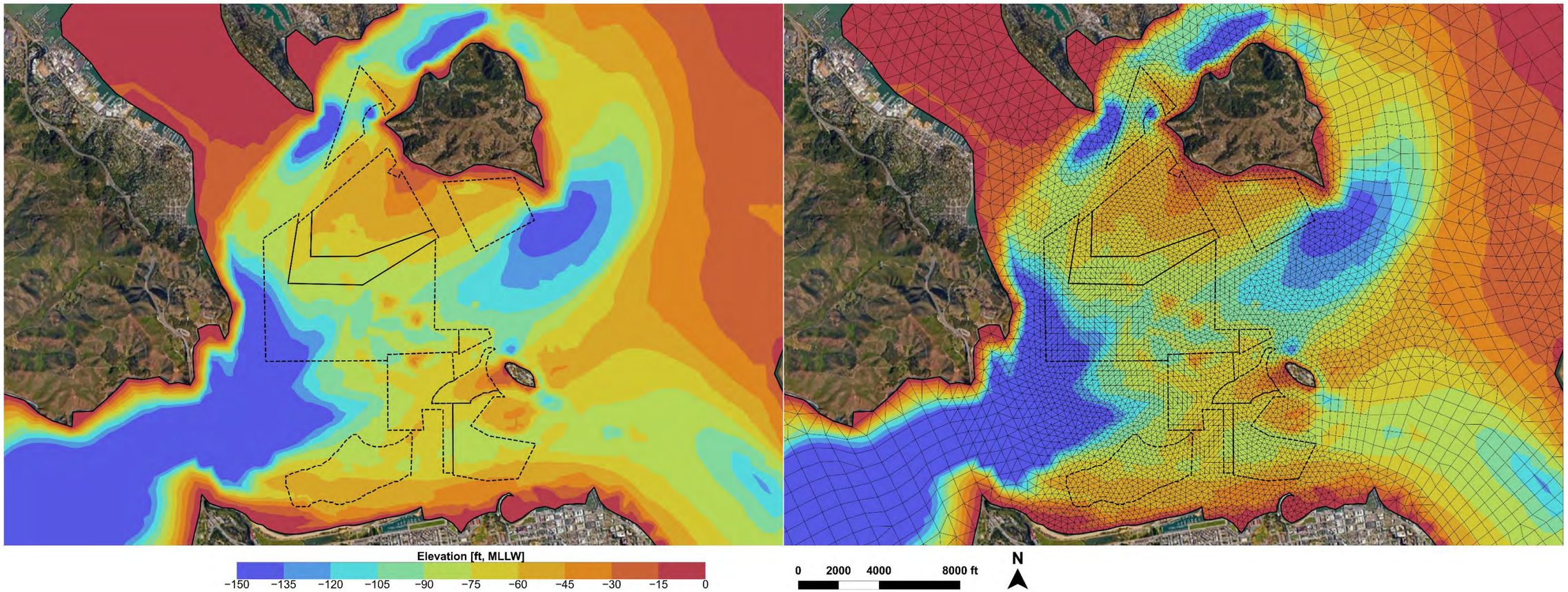

Notes:

1. Elevations shown for Existing Conditions in Central Bay based on the 2019 multibeam hydrographic survey (eTrac 2019).

Figure 2.3:

Modeling Domain Close-up (Left) and Grid (Right) in Central Bay

COAST & HARBOR ENGINEERING

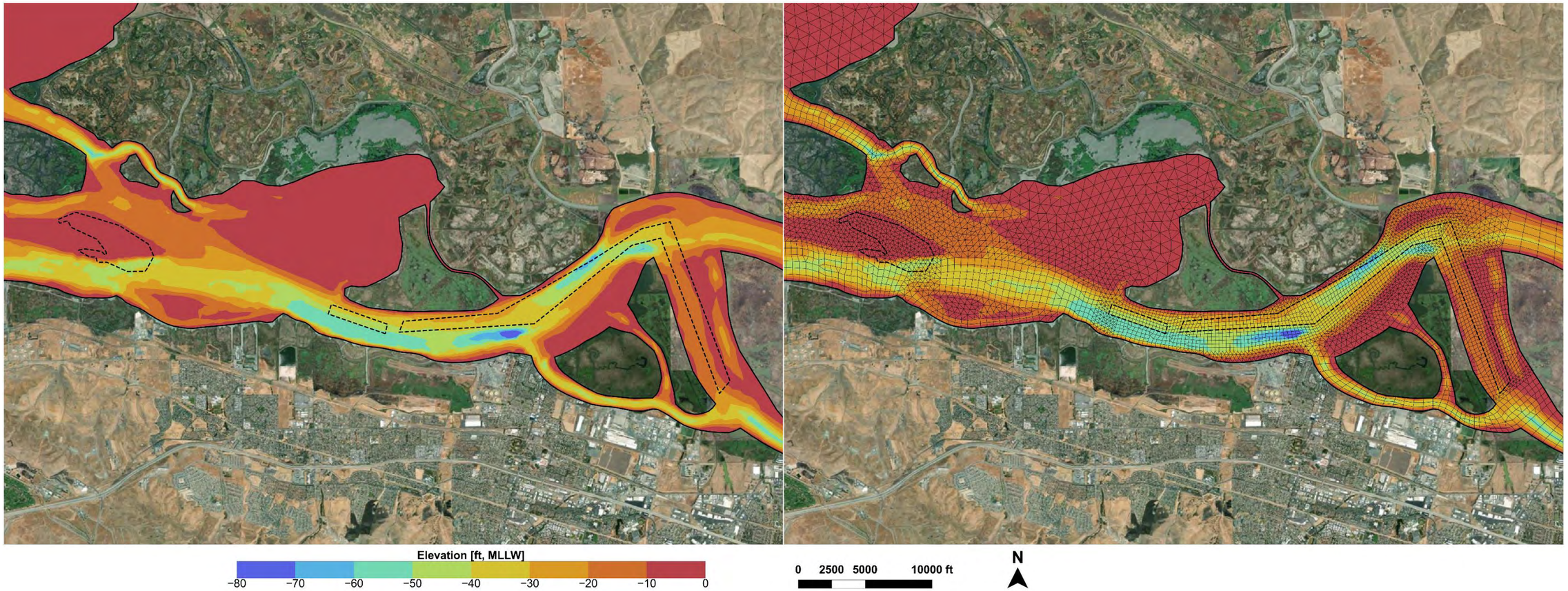

Notes:

1. Elevations shown for Existing Conditions in Suisun Bay based on the 2019 multibeam hydrographic survey (eTrac 2019).

Figure 2.4:

Modeling Domain Close-up (Left) and Grid (Right) in Suisun Bay

COAST & HARBOR ENGINEERING

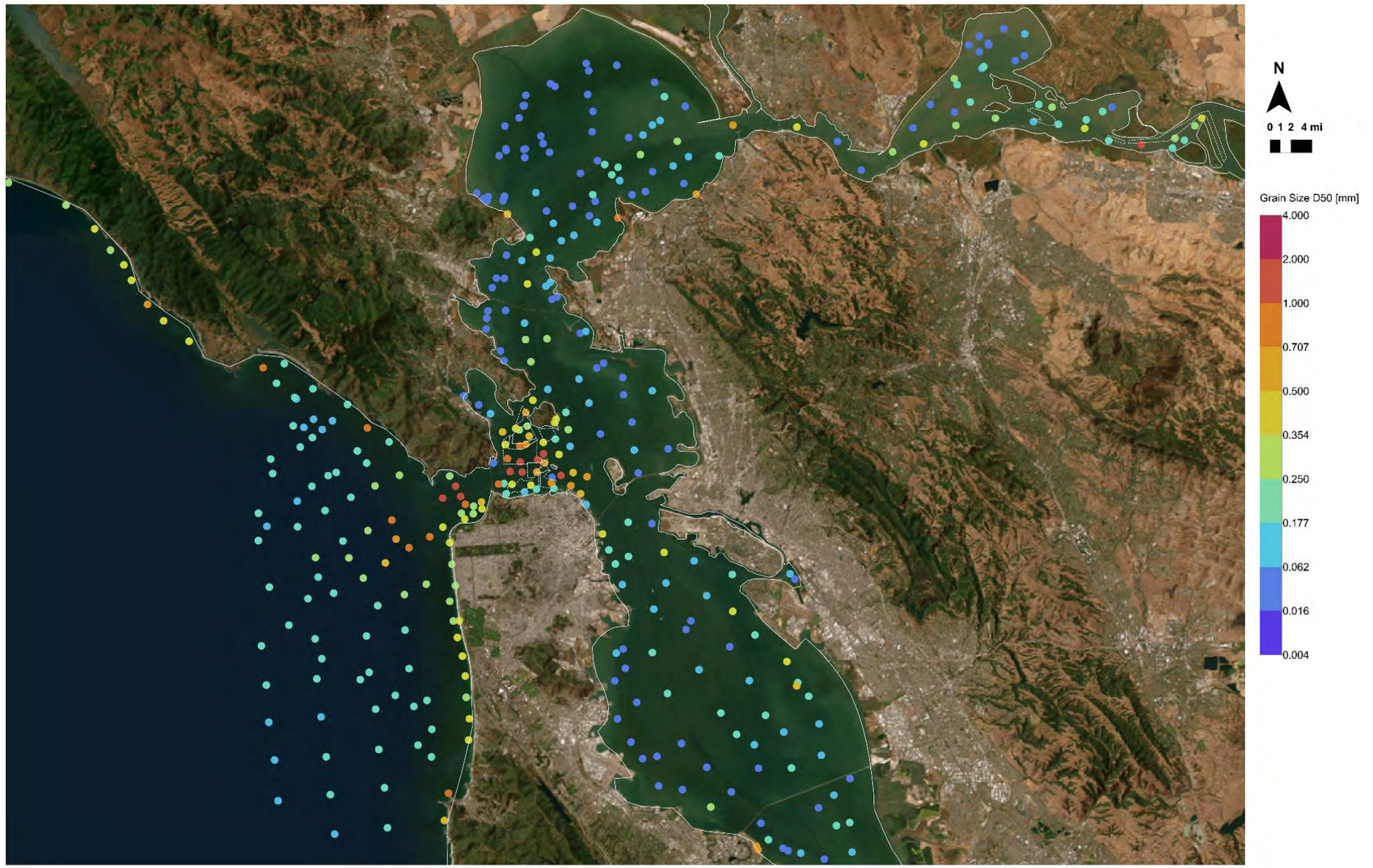

Notes:

1. Points represent locations of sediment samples incorporated into the modeling domain (see text Section 2.5 for data sources). Grain size data for the lease areas from 2022 quarterly mining reports provided by CSLC are not shown.
2. Colors represent measured median grain diameter.

Figure 2.5:

Measured Grain Size Inputs

COAST & HARBOR ENGINEERING

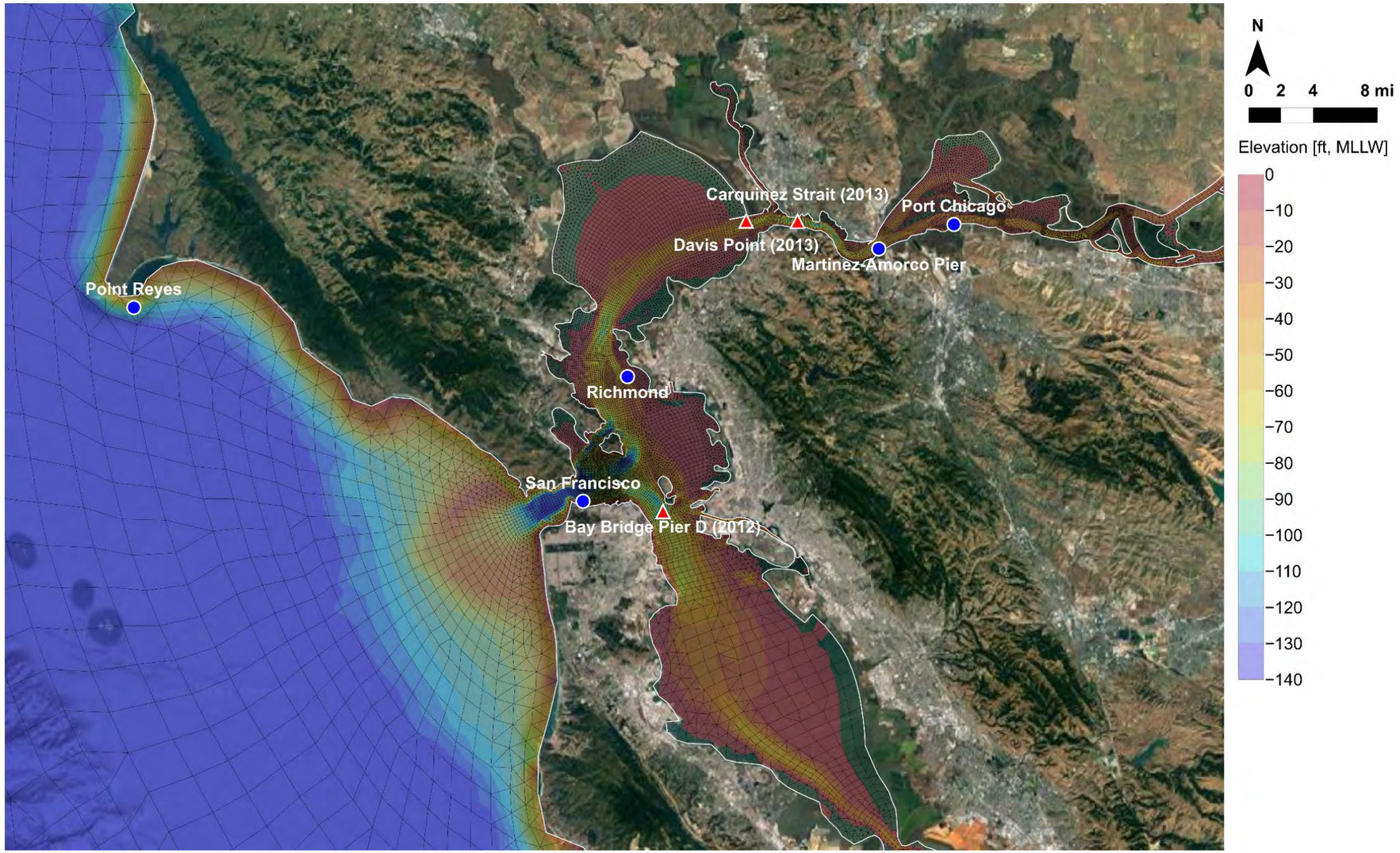

Notes:

1. Blue circles represent locations where NOAA predicted tides were compared with model results.
2. Red triangles represent locations where bottom-mounted ADCPs were positioned by NOAA, in the years noted. Data include velocities at multiple vertical bins in the water column.

Figure 2.6:

Validation Locations

COAST & HARBOR ENGINEERING

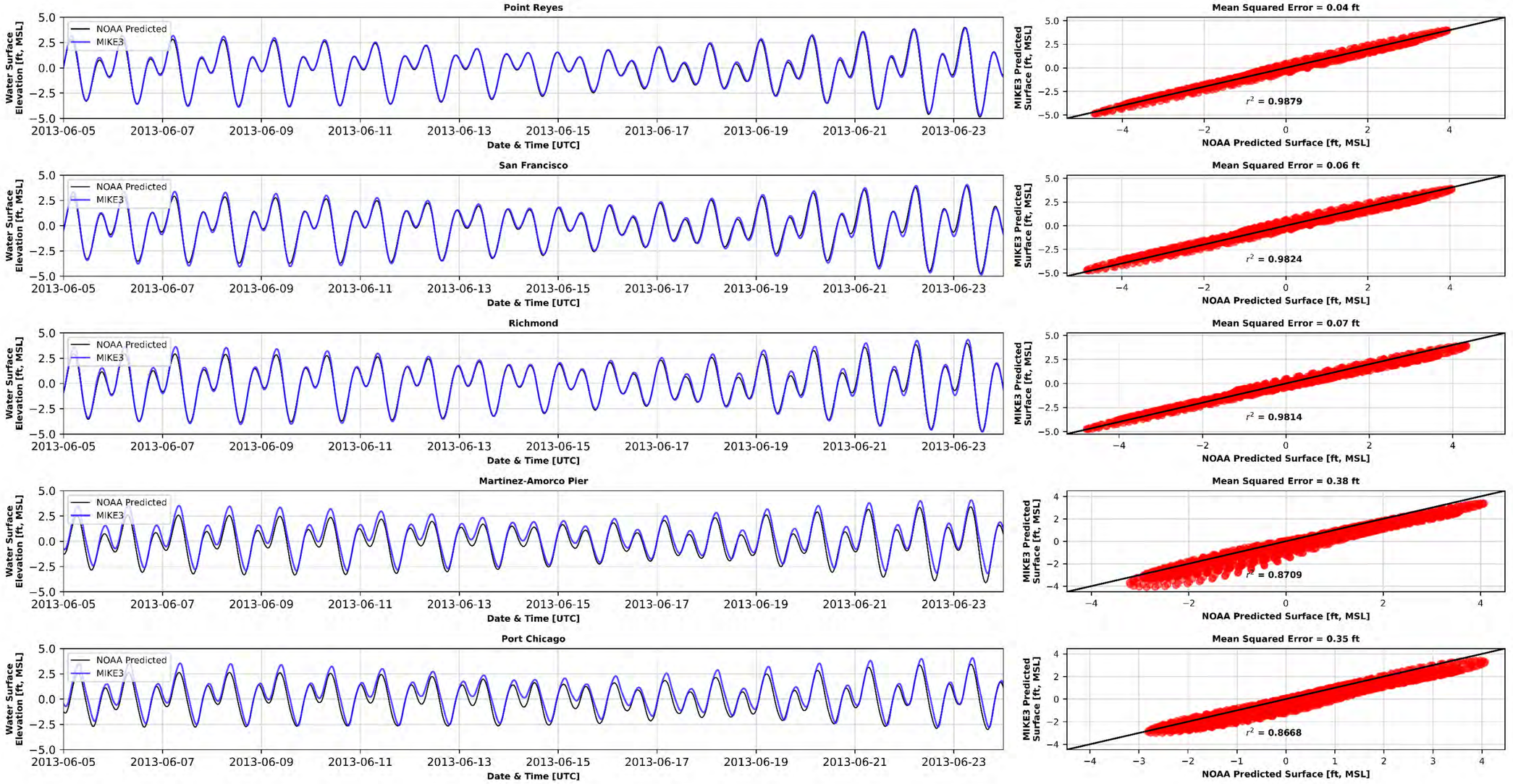

Notes:

1. NOAA tides compared with model results are predicted tides.

Figure 2.7:

Water Surface Elevation Validations

COAST & HARBOR ENGINEERING

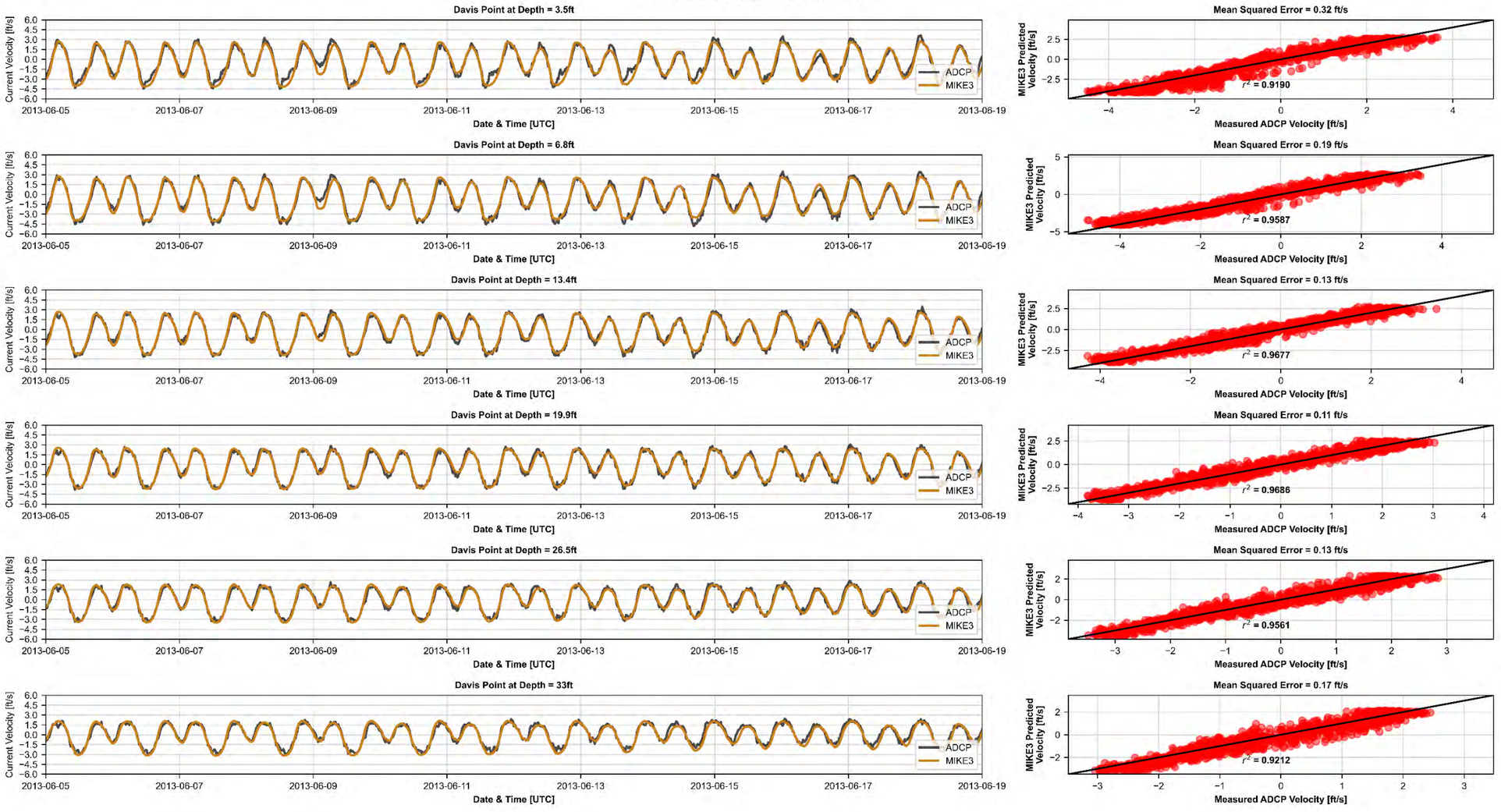

Notes:

1. Top panel compares model results with near-bottom current velocities. Bottom panel compares model results with near-surface current velocities.
2. Negative current velocities represent ebb currents.

Figure 2.8:

Current Velocity Validation at Davis Point

COAST & HARBOR ENGINEERING

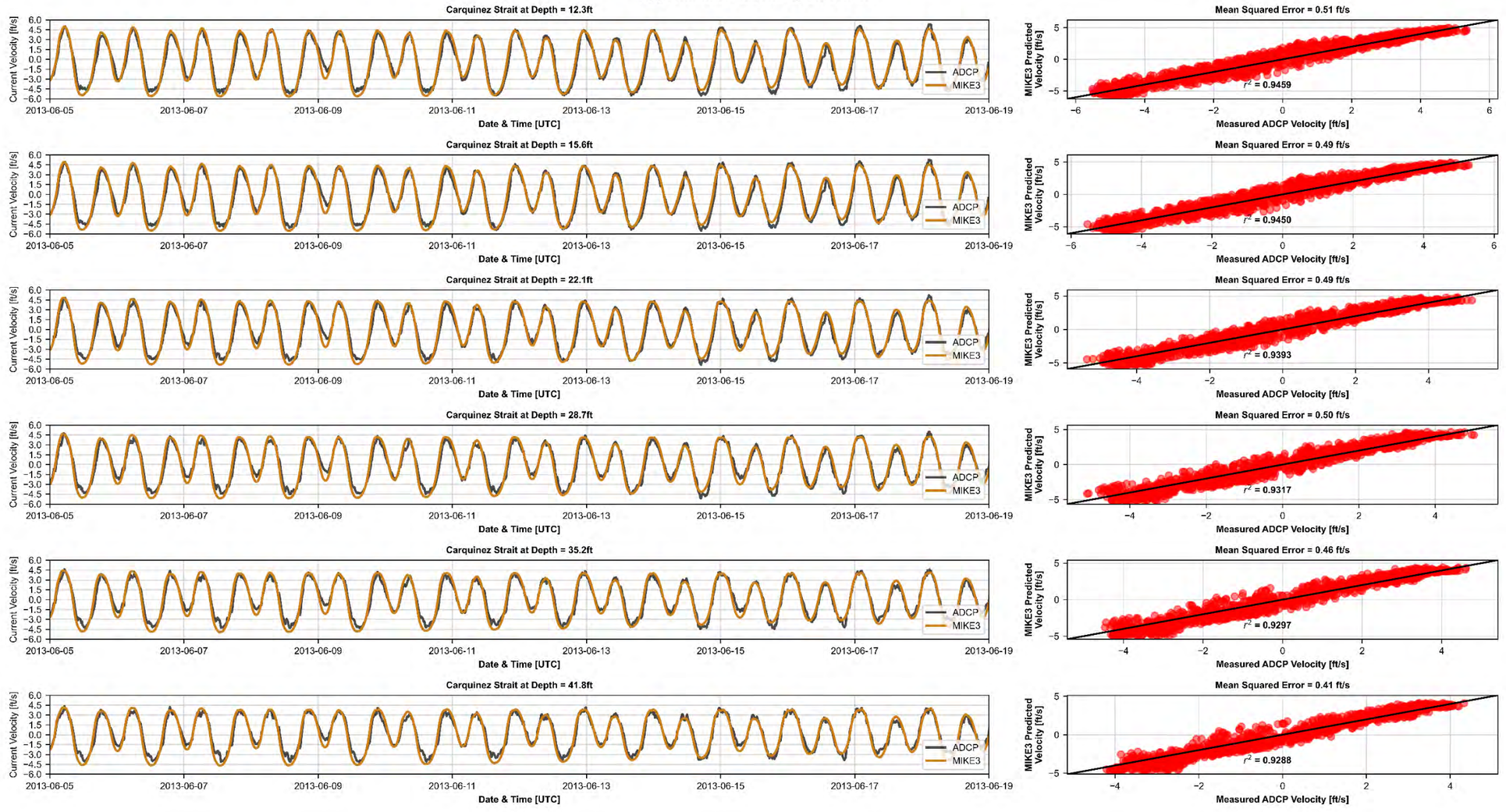

Notes:

1. Top panel compares model results with near-bottom current velocities. Bottom panel compares model results with near-surface current velocities.
2. Negative current velocities represent ebb currents.

Figure 2.9:

Current Velocity Validation at Carquinez Strait

COAST & HARBOR ENGINEERING

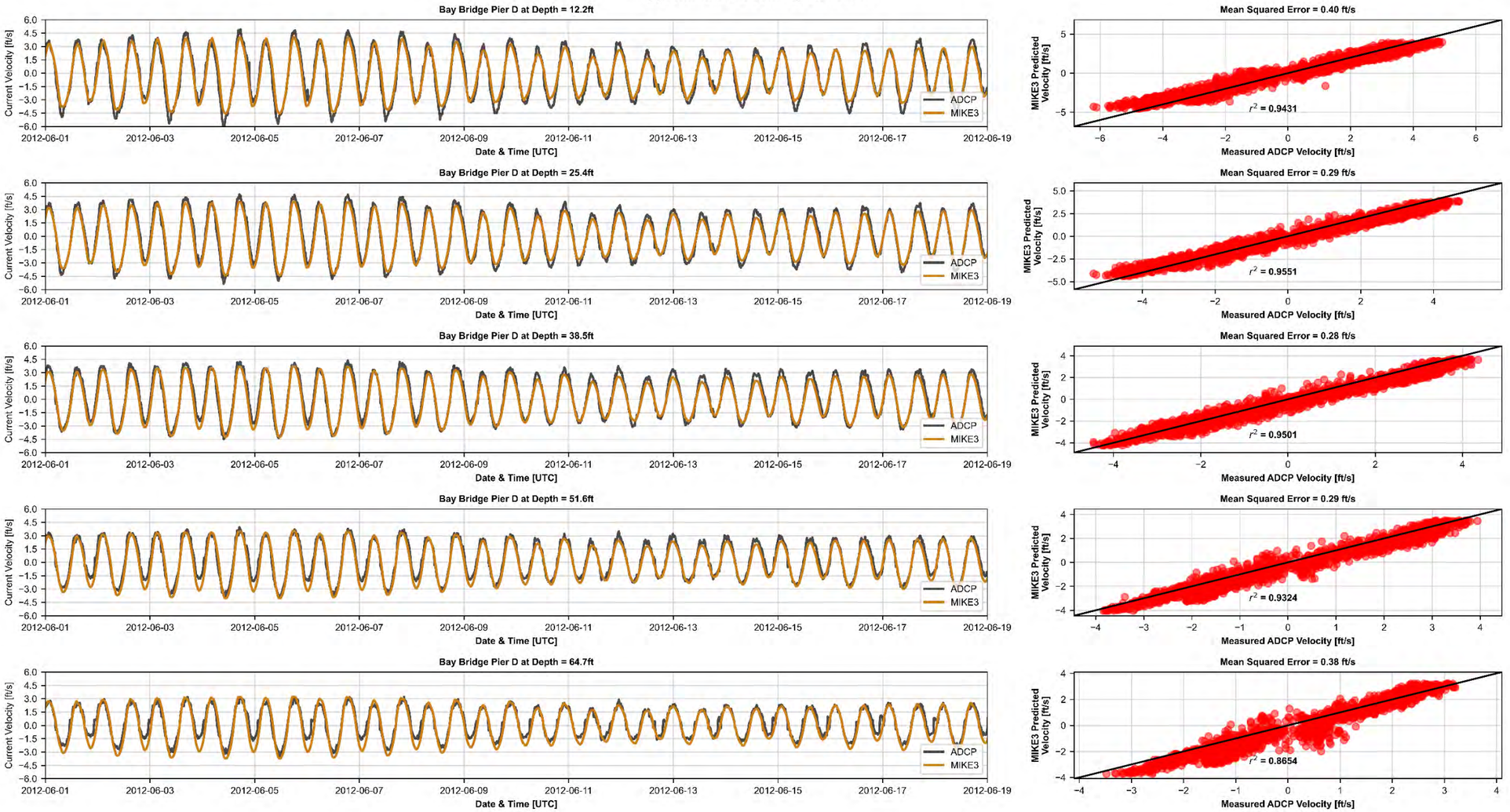

Notes:

1. Top panel compares model results with near-bottom current velocities. Bottom panel compares model results with near-surface current velocities.
2. Negative current velocities represent ebb currents.

Figure 2.10:

Current Velocity Validation at Bay Bridge Pier D

COAST & HARBOR ENGINEERING

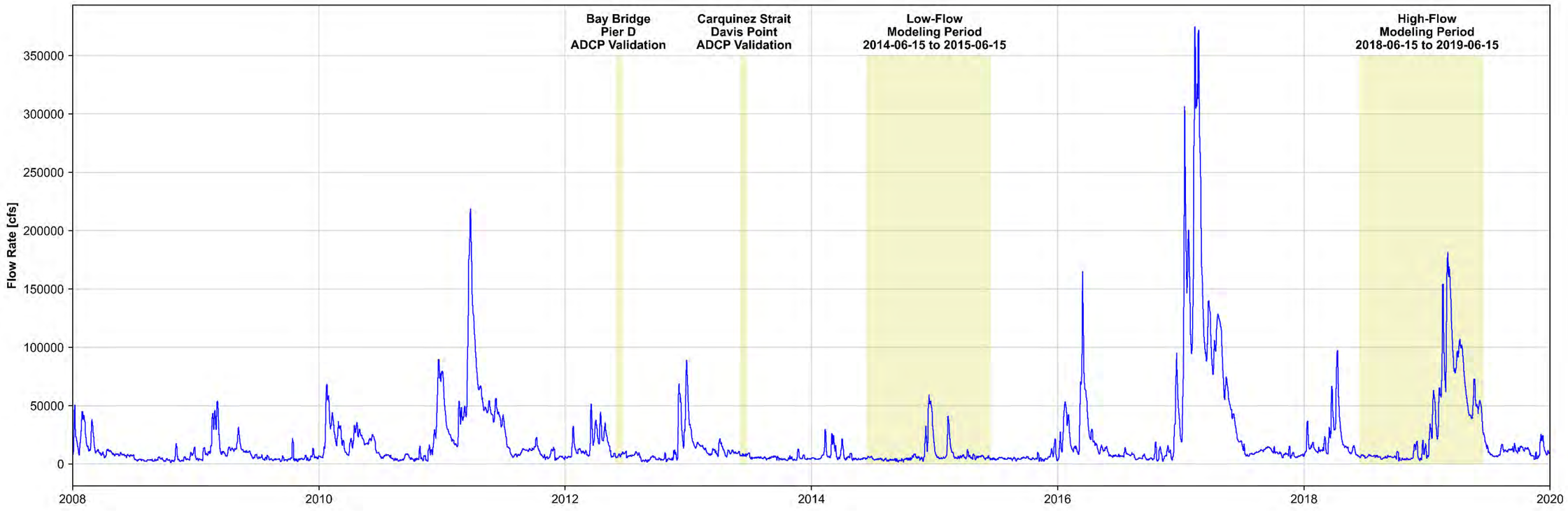

Notes:

1. Total Delta outflow data were taken from DAYFLOW model results.

Figure 2.11:

Simulation Periods and Delta Outflow Boundary Conditions

COAST & HARBOR ENGINEERING

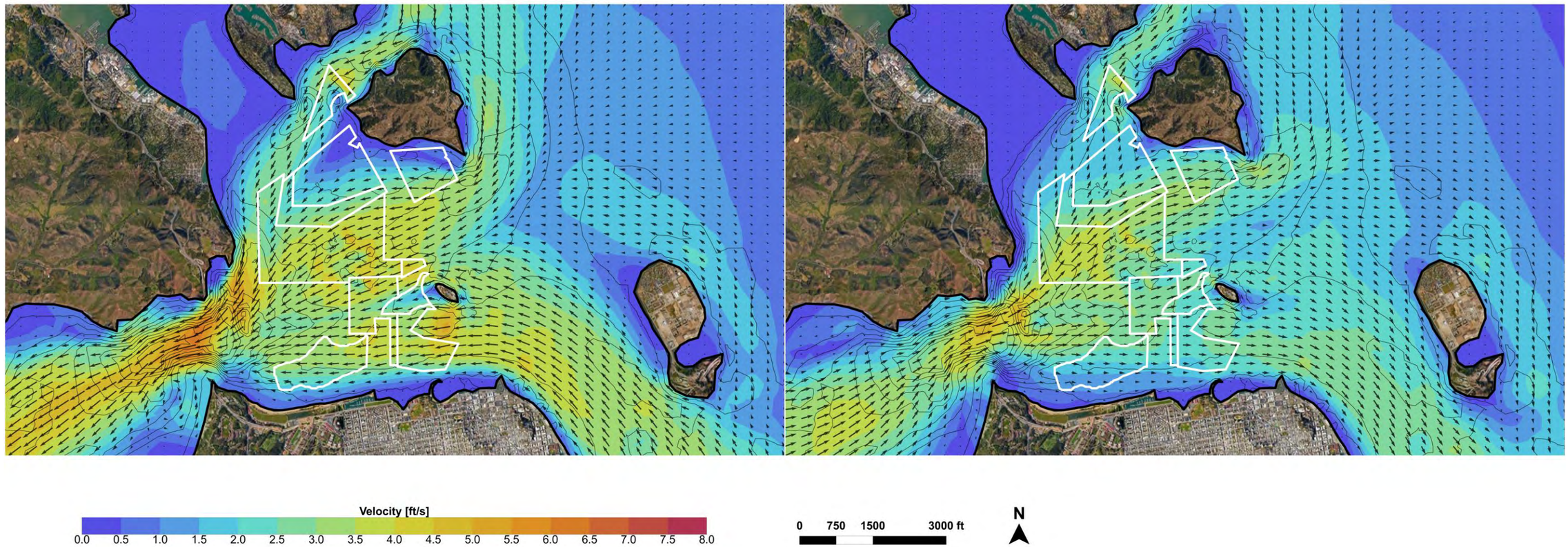

Notes:

1. Current velocities shown above were taken from the bottom vertical cells in the modeling results.

Figure 3.1:

Peak Ebb (Left) and Flood (Right) Near-Bottom Currents in Central Bay

COAST & HARBOR ENGINEERING

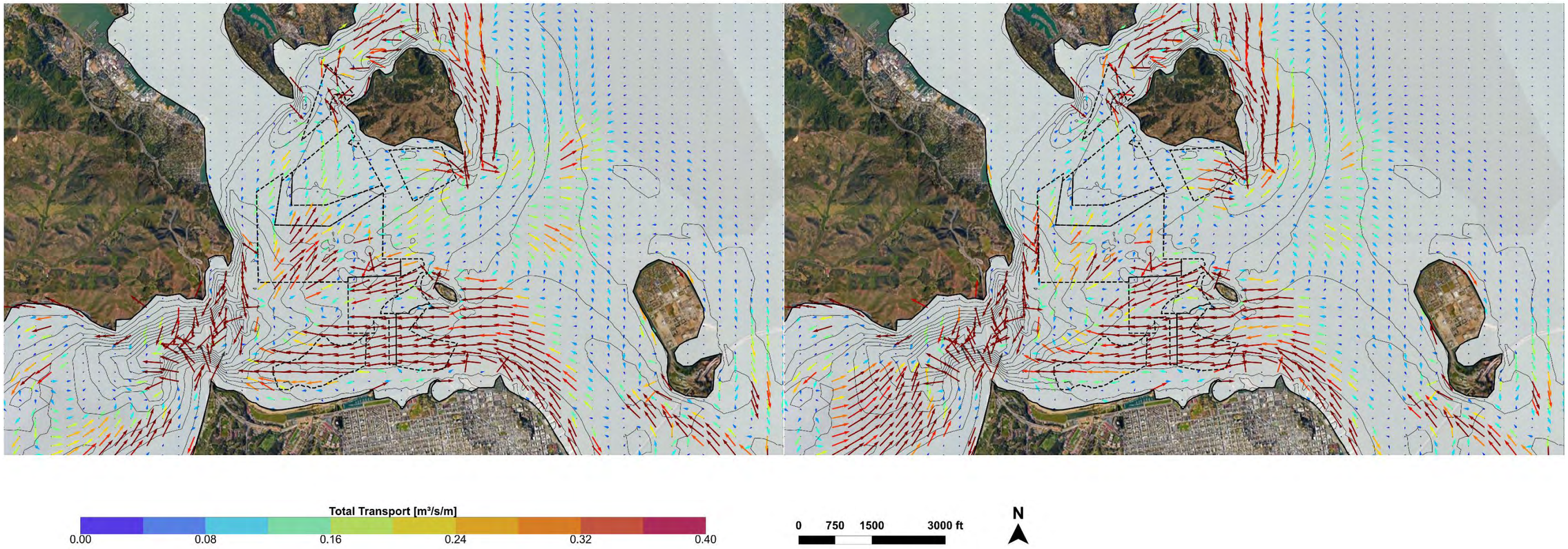

Notes:

1. Vectors depict direction and magnitude of net total sand transport computed over one-year simulations. Vector length and color both represent magnitude of net total sand transport.

Figure 3.2:

One-Year Net Total Transport for Low-Flow Simulation (Left) and High-Flow Simulation (Right) in Central Bay

COAST & HARBOR ENGINEERING

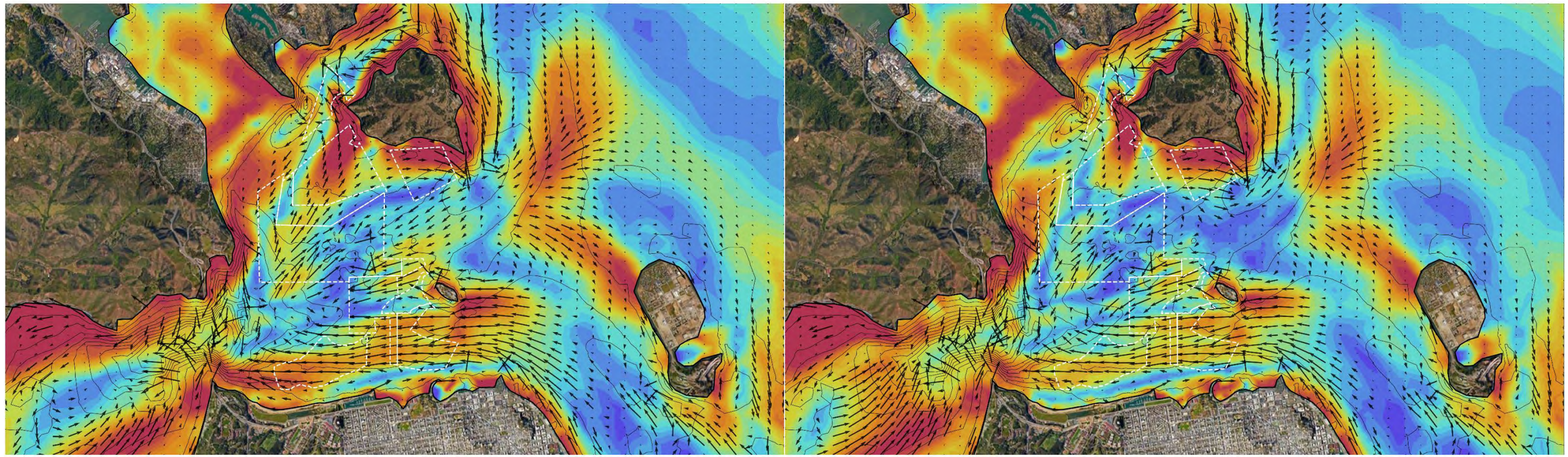

Notes:

1. Vectors depict direction and magnitude of net total sand transport computed over one-year simulations for Existing Conditions.

Figure 3.3:

One-Year Net Total Transport as a Percentage of Gross Total Transport for Low-Flow Simulation (Left) and High-Flow Simulation (Right) in Central Bay

COAST & HARBOR ENGINEERING

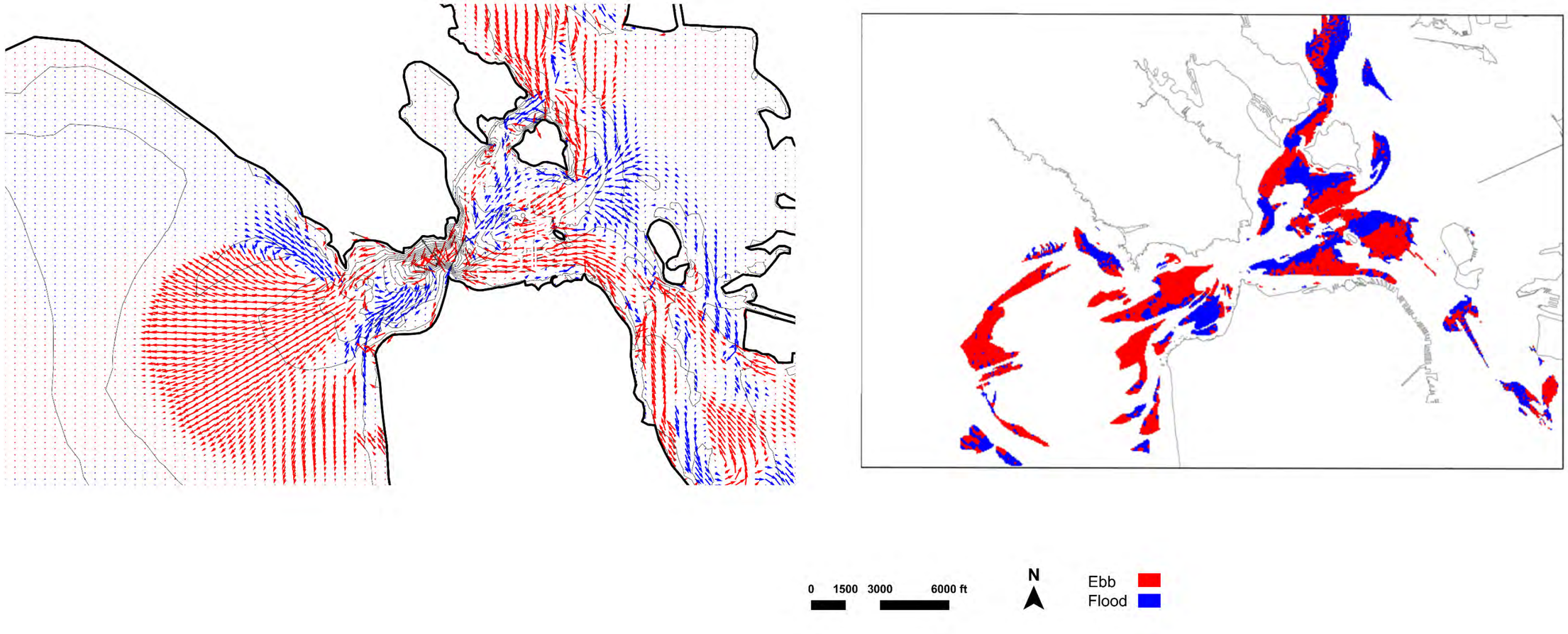

Notes:

1. Predicted net total transport vectors (left) colored approximately by flow direction (ebb in red, flood in blue) to facilitate comparison with transport directions inferred from bedforms (right).
2. Vectors showing predicted net total transport (left) are scaled in length according to transport magnitude.

Figure 3.4:

Comparison of Predicted Net Total Transport from Low-Flow Simulation (Left) and Transport Directions Inferred from Bedforms (Right, Barnard et al. 2013)

COAST & HARBOR ENGINEERING

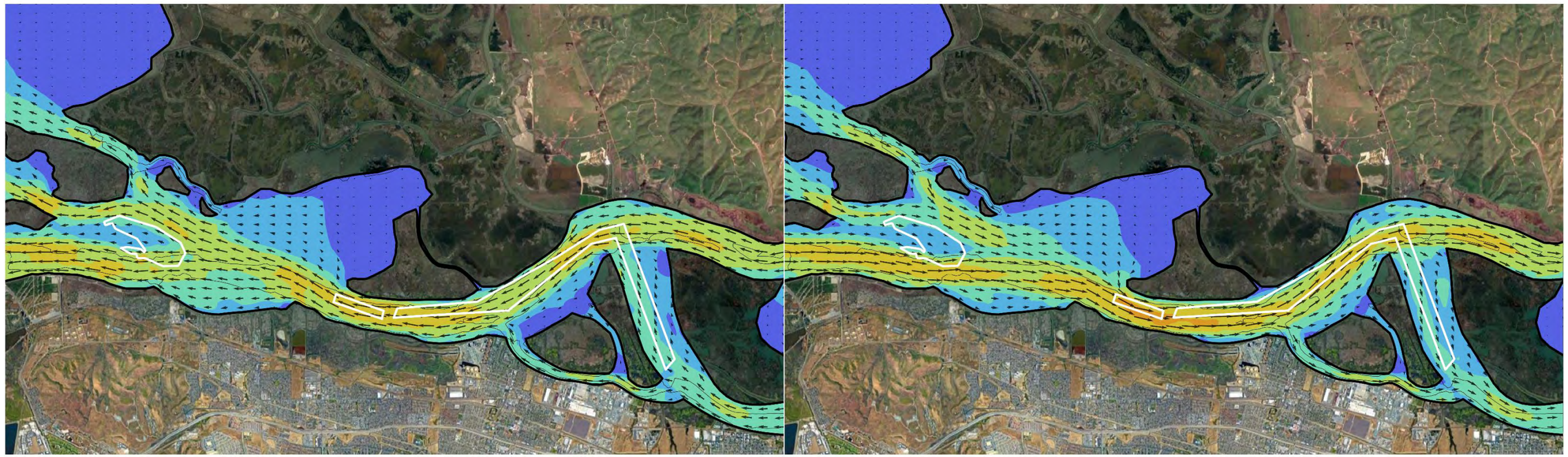

Notes:

1. Current velocities shown above were taken from the bottom vertical cells in the modeling results.

Figure 3.5:

Peak Ebb (Left) and Flood (Right) Near-Bottom Currents in Suisun Bay

COAST & HARBOR ENGINEERING

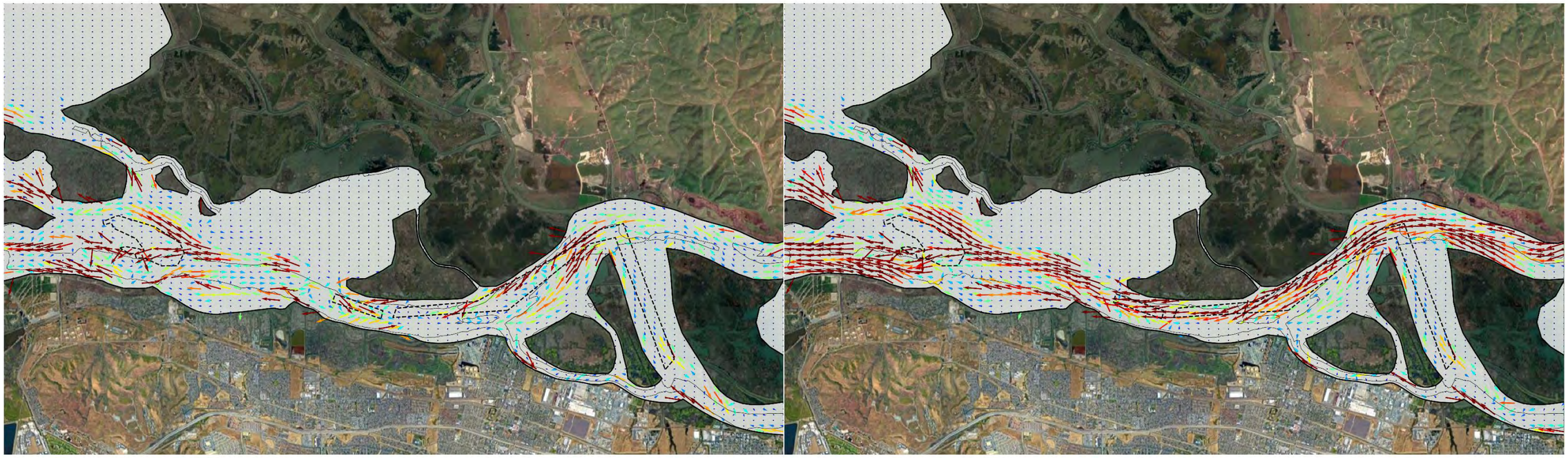

Notes:

1. Vectors depict direction and magnitude of net total sand transport computed over one-year simulations. Vector length and color both represent magnitude of net total sand transport.

Figure 3.6:

One-Year Net Total Transport for Low-Flow Simulation (Left) and High-Flow Simulation (Right) in Suisun Bay

COAST & HARBOR ENGINEERING

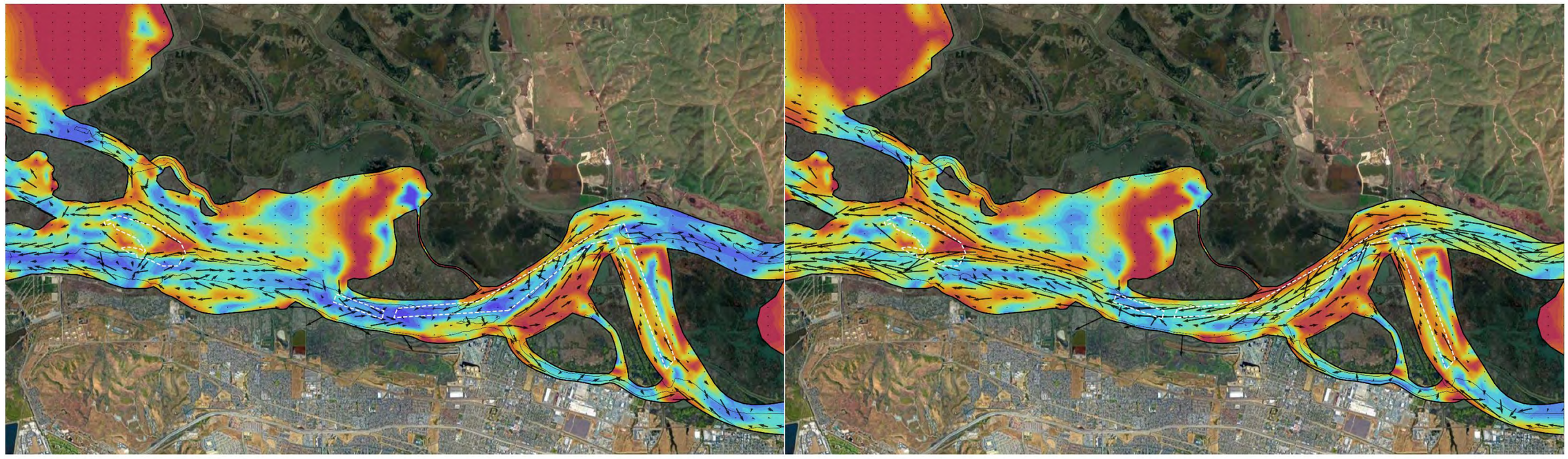

Notes:

1. Vectors depict direction and magnitude of net total sand transport computed over one-year simulations for Existing Conditions.

Figure 3.7:

One-Year Net Total Transport as a Percentage of Gross Total Transport for Low-Flow Simulation (Left) and High-Flow Simulation (Right) in Suisun Bay

COAST & HARBOR ENGINEERING

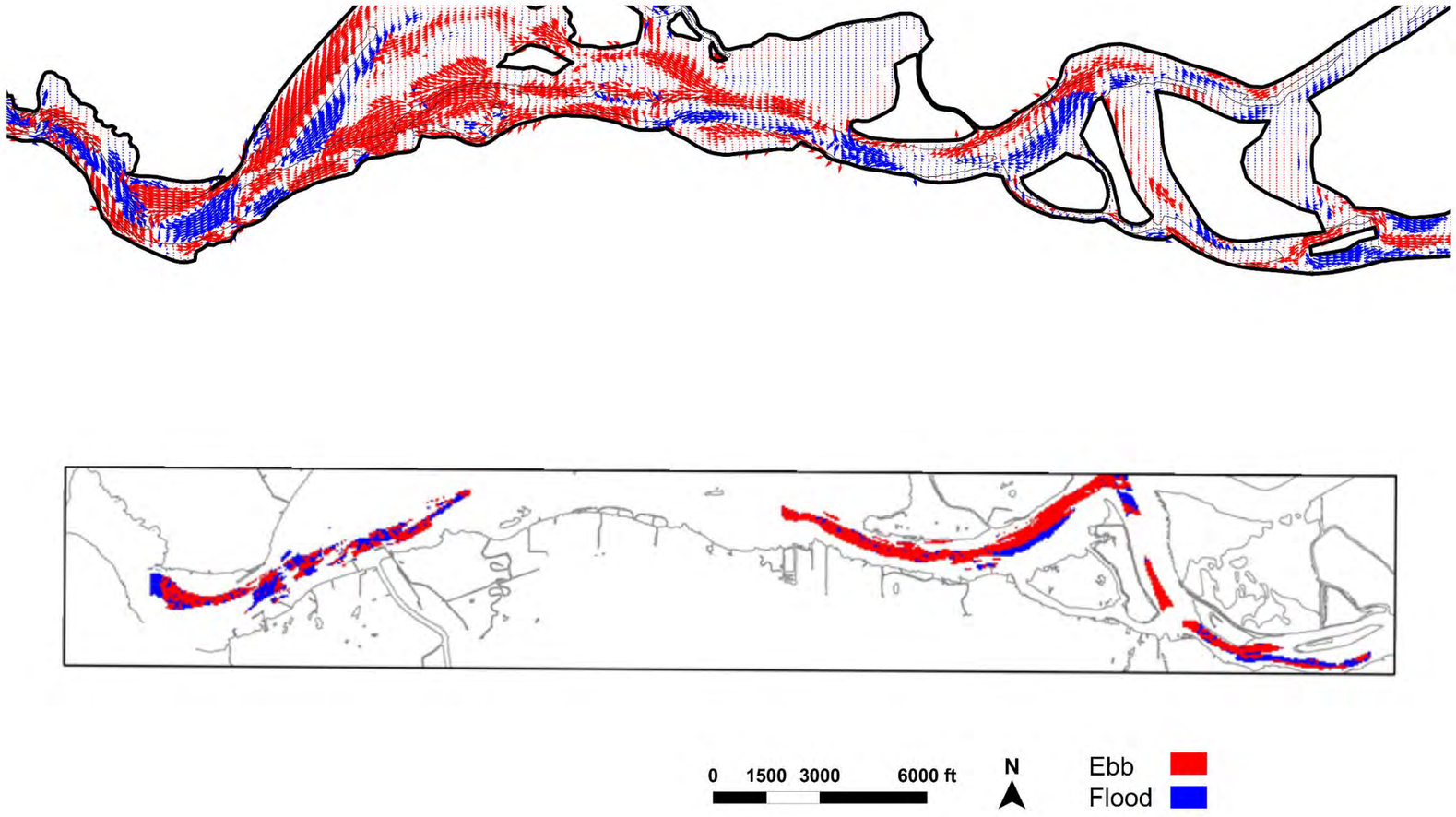

Notes:

1. Predicted net total transport vectors (left) colored approximately by flow direction (ebb in red, flood in blue) to facilitate comparison with transport directions inferred from bedforms (right).
2. Vectors showing predicted net total transport vectors (left) scaled in length according to transport magnitude.

Figure 3.8:

Comparison of Predicted Net Total Transport from Low-Flow Simulation (Top) and Transport Directions Inferred from Bedforms (Bottom, Barnard et al. 2013)

COAST & HARBOR ENGINEERING

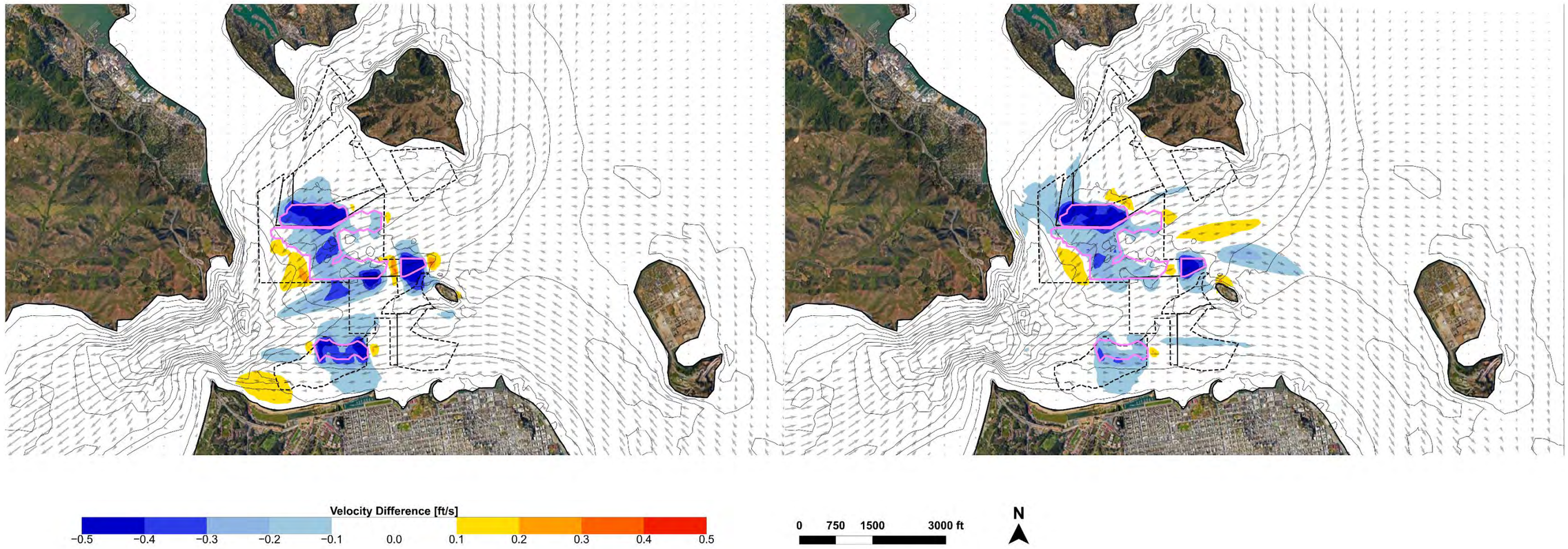

Notes:

1. Current speed differences were calculated by subtracting current speed predicted for Proposed Mining from current speed predicted for No Proposed Mining, at a single model time step.
2. Current speeds for Proposed Mining and No Proposed Mining taken at bottom vertical layer.
3. Magenta polygons represent the mining areas that were deepened within the lease areas.

Figure 4.1:

Near-Bottom Current Speed Differences Caused by Proposed Mining Relative to No Proposed Mining During Peak Ebb (Left) and Flood (Right) Currents During Low-Flow Simulation, in Central Bay

COAST & HARBOR ENGINEERING

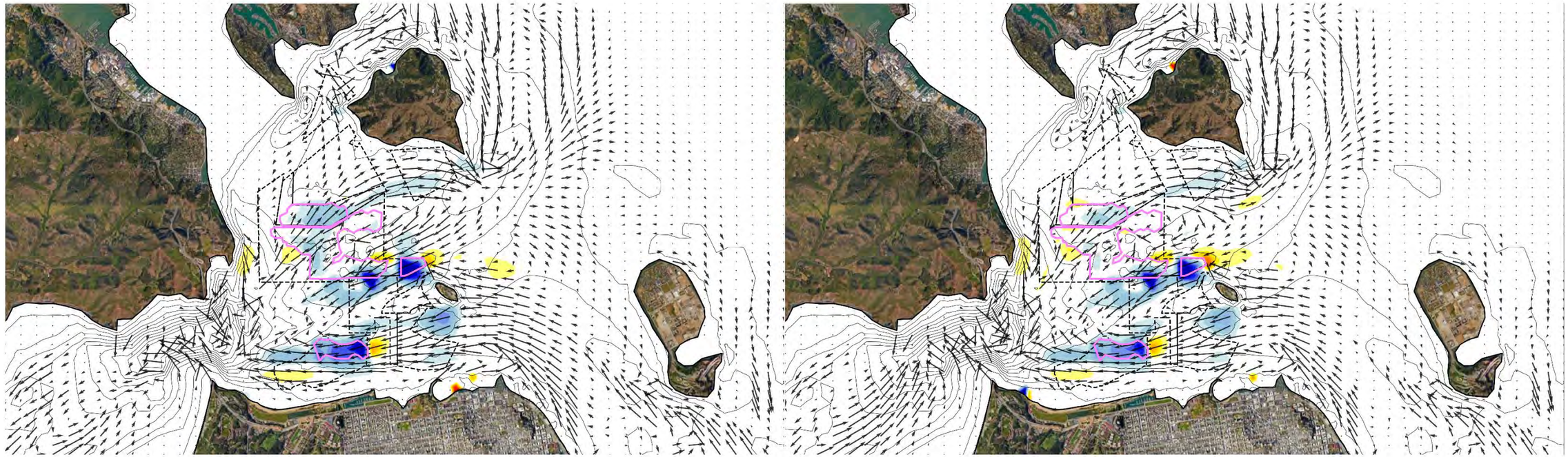

Notes:

1. Vectors represent net total sand transport predicted for No Proposed Mining.
2. Total transport difference computed by subtracting net total transport for Proposed Mining from net total transport for No Proposed Mining.
3. Magenta polygons represent the mining areas that were deepened within the lease areas.

Figure 4.2:

One-Year Net Total Transport Changes Caused by Proposed Mining Relative to No Proposed Mining for Low-Flow (Left) and High-Flow (Right) Simulations in Central Bay

COAST & HARBOR ENGINEERING

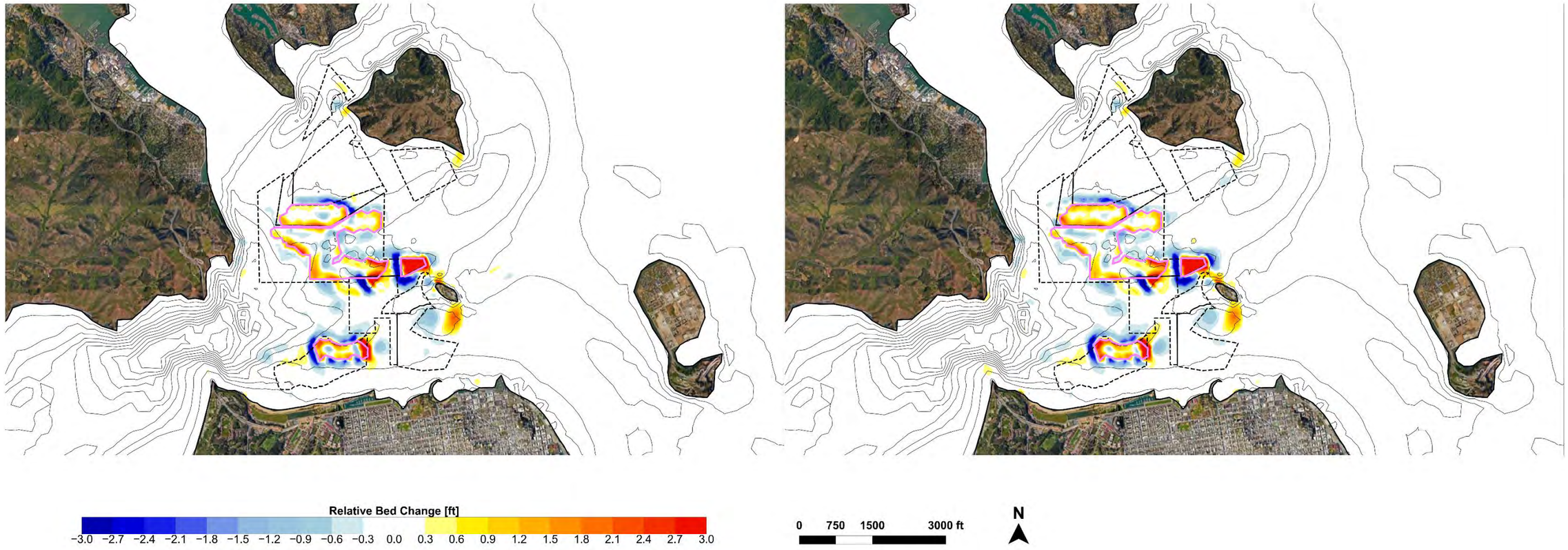

Notes:

1. Relative Bed Change was calculated by subtracting bed changes predicted for Proposed Mining from bed changes predicted for No Proposed Mining.
2. Magenta polygons represent the mining areas that were deepened within the lease areas.

Figure 4.3:

One-Year Bed Change Differences Caused by Proposed Mining Relative to No Proposed Mining for Low-Flow (Left) and High-Flow (Right) Simulations in Central Bay

COAST & HARBOR ENGINEERING

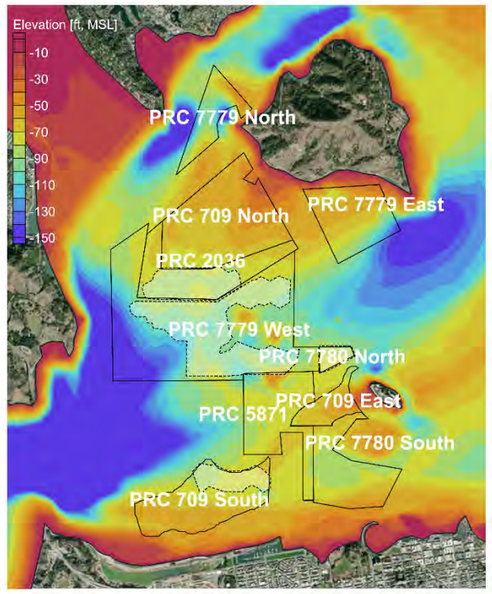

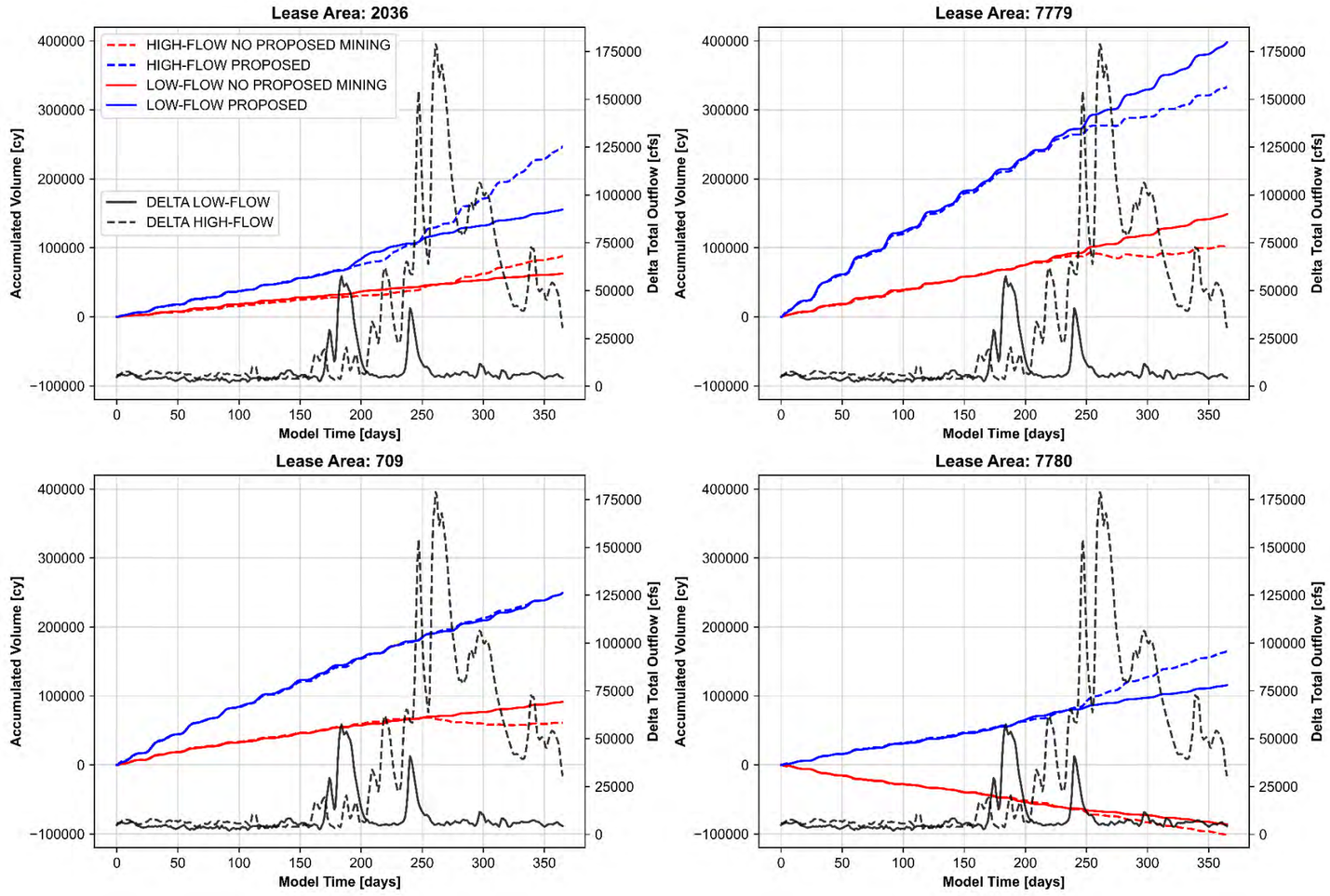

Notes:

1. Cumulative volumetric changes were calculated within the deepened zone of the lease areas only (shaded white at left), starting after the full 10-year mining volumes were removed.

Figure 4.4:

Volumetric Trends of Erosion and Deposition in Deepened Zones of the Lease Areas During Low-Flow and High-Flow Simulations in Central Bay

COAST & HARBOR ENGINEERING

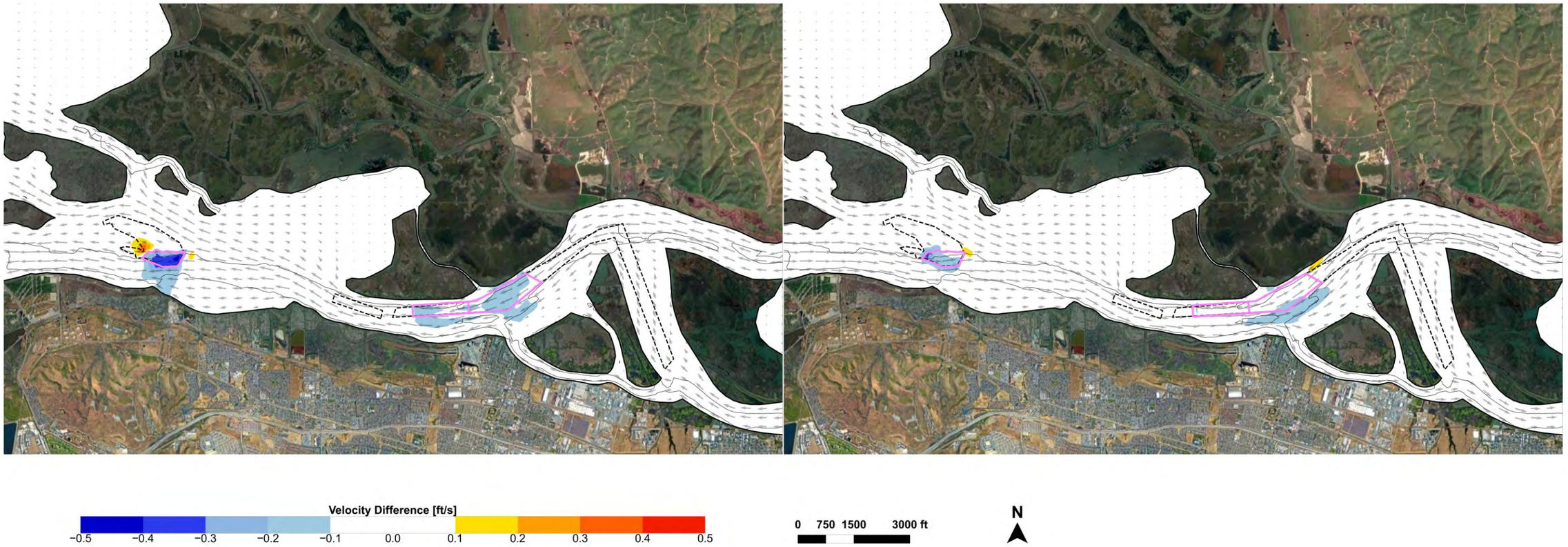

Notes:

1. Current speed differences were calculated by subtracting current speed predicted for Proposed Mining from current speed predicted for No Proposed Mining, at a single model time step.
2. Current speeds for No Proposed Mining and Proposed Mining taken at bottom vertical layer.
3. Magenta polygons represent the mining areas that were deepened within the lease areas.

Figure 4.5:

Near-Bottom Current Speed Differences Caused by Proposed Mining Relative to No Proposed Mining During Peak Ebb (Left) and Flood (Right) Currents During Low-Flow Simulation, in Suisun Bay

COAST & HARBOR ENGINEERING

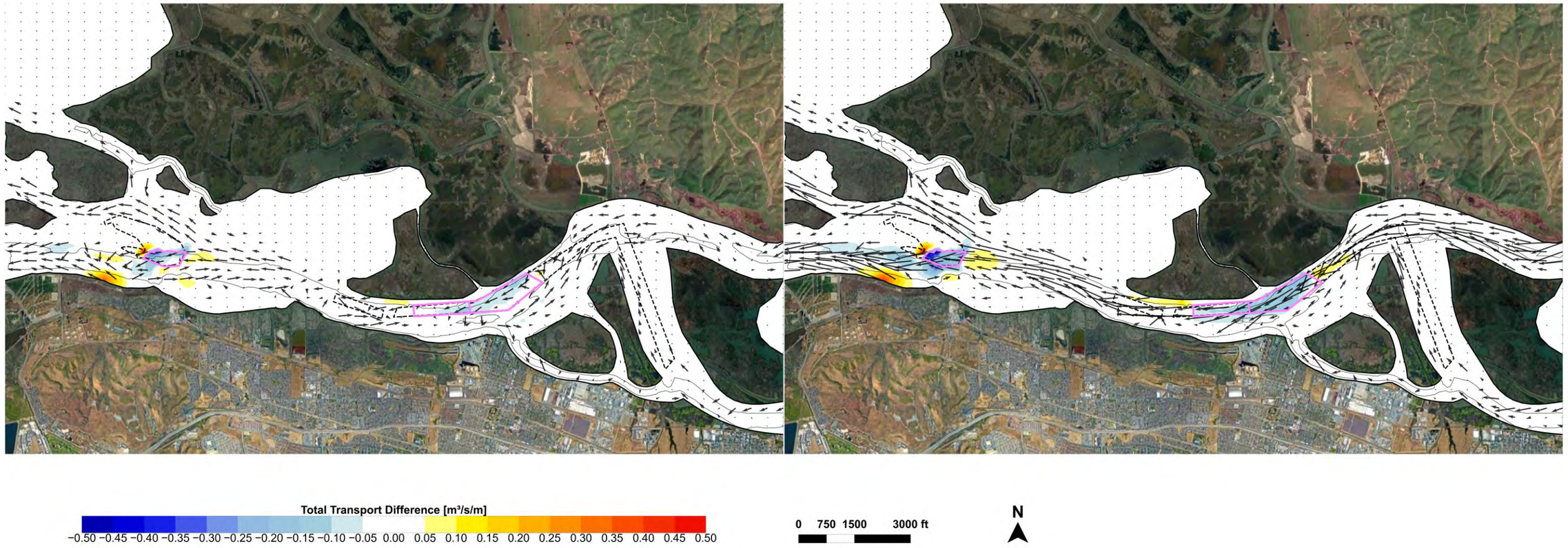

Notes:

1. Vectors represent net total sand transport predicted for No Proposed Mining.
2. Total transport difference computed by subtracting net total transport for Proposed Mining from net total transport for No Proposed Mining.

Figure 4.6:

One-Year Net Total Transport Changes Caused by Proposed Mining Relative to No Proposed Mining for Low-Flow (Left) and High-Flow (Right) Simulations in Suisun Bay

COAST & HARBOR ENGINEERING

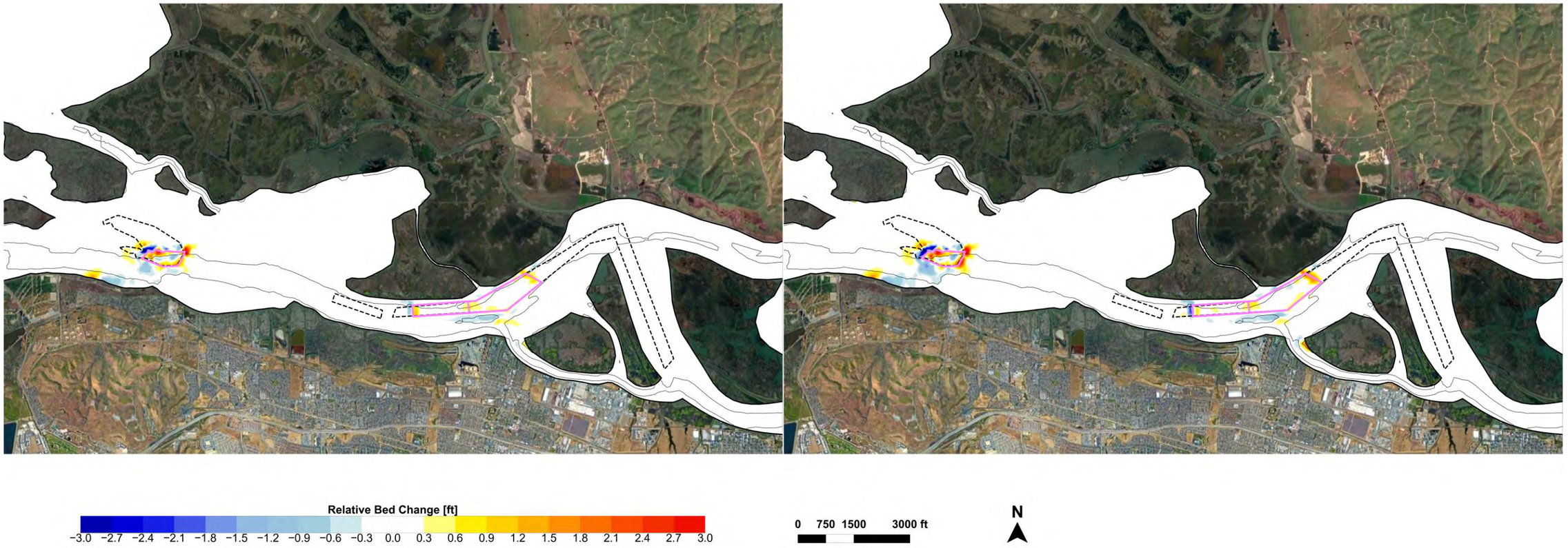

Notes:

1. Relative Bed Change was calculated by subtracting bed changes predicted for Proposed Mining from bed changes predicted for No Proposed Mining.

Figure 4.7:

One-Year Bed Change Differences Caused by Proposed Mining Relative to No Proposed Mining for Low-Flow (Left) and High-Flow (Right) Simulations in Suisun Bay

COAST & HARBOR ENGINEERING

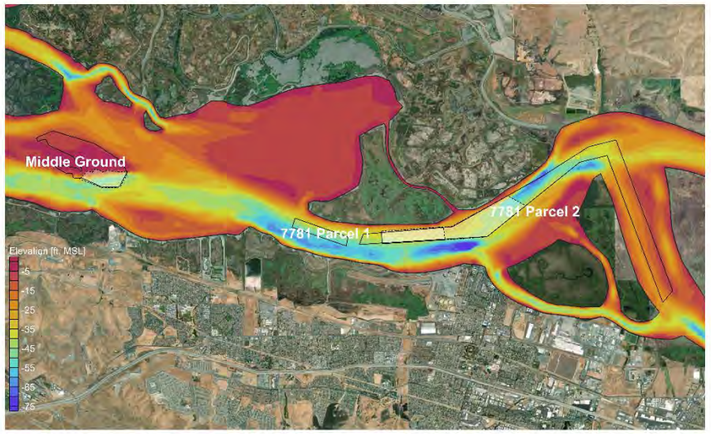

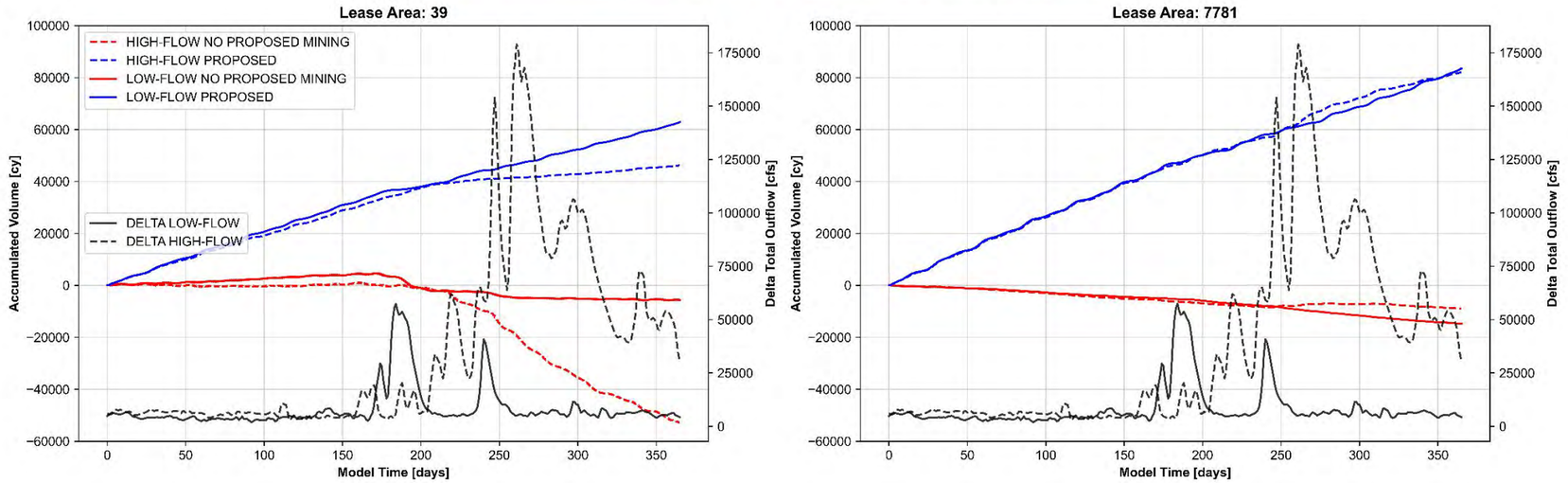

Notes:

1. Cumulative volumetric changes were calculated within the deepened zone of the lease areas only (shaded white at top), starting after the full 10-year mining volumes were removed.
2. Areas deepened to represent mining in Lease Area 7781 East are different for Proposed Mining and No Proposed Mining.

Figure 4.8:

Volumetric Trends of Erosion and Deposition in Deepened Zones of the Lease Areas During Low-Flow and High-Flow Simulations in Suisun Bay

COAST & HARBOR ENGINEERING

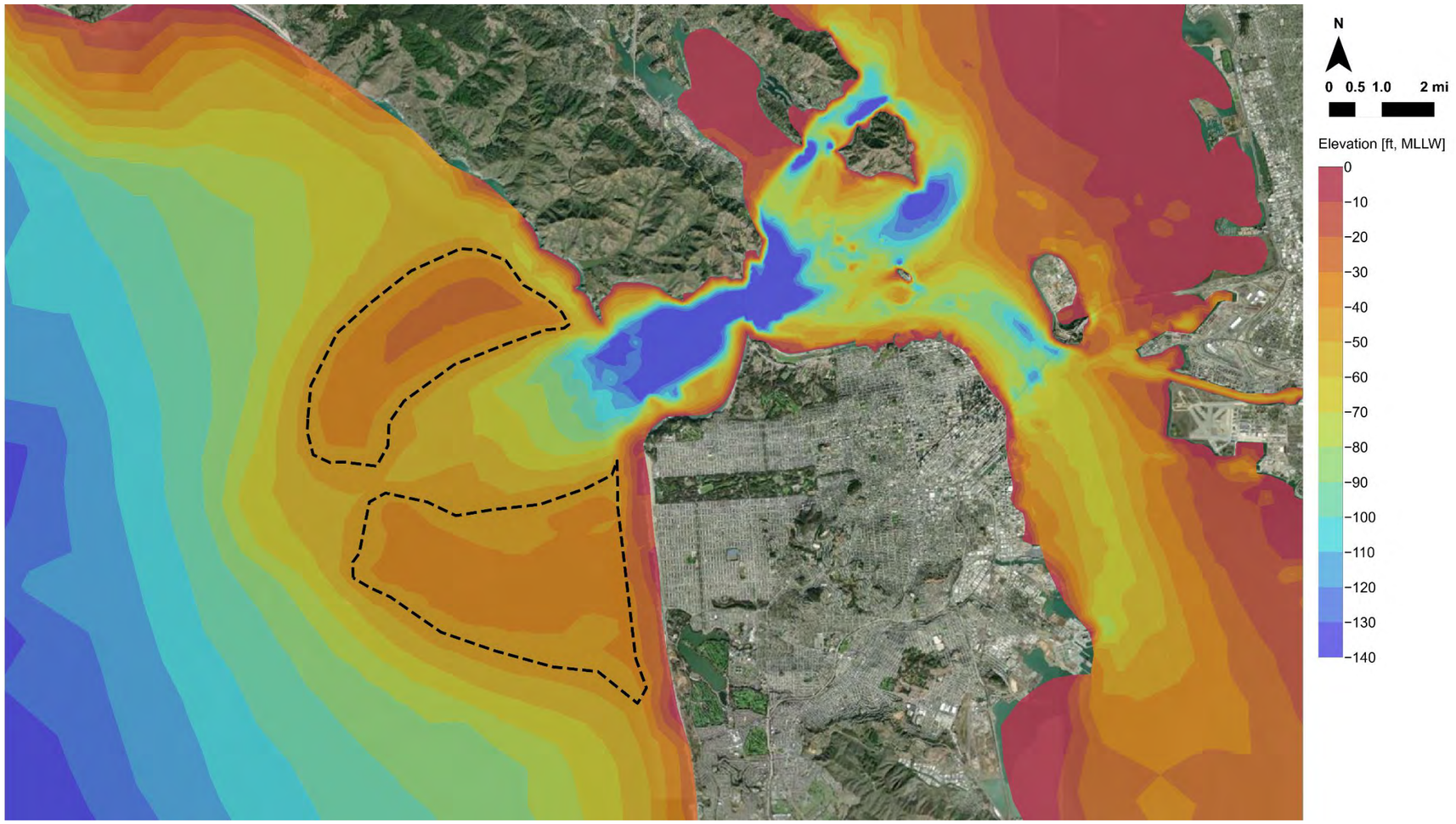

Notes:

1. Area for volume calculations is approximately delineated by elevations above -45 feet (MLLW) except near Ocean Beach.

Figure 4.9:

Area on the San Francisco Bar Evaluated for Changes in Sand Volume Caused by Proposed Mining Relative to No Proposed Mining

COAST & HARBOR ENGINEERING

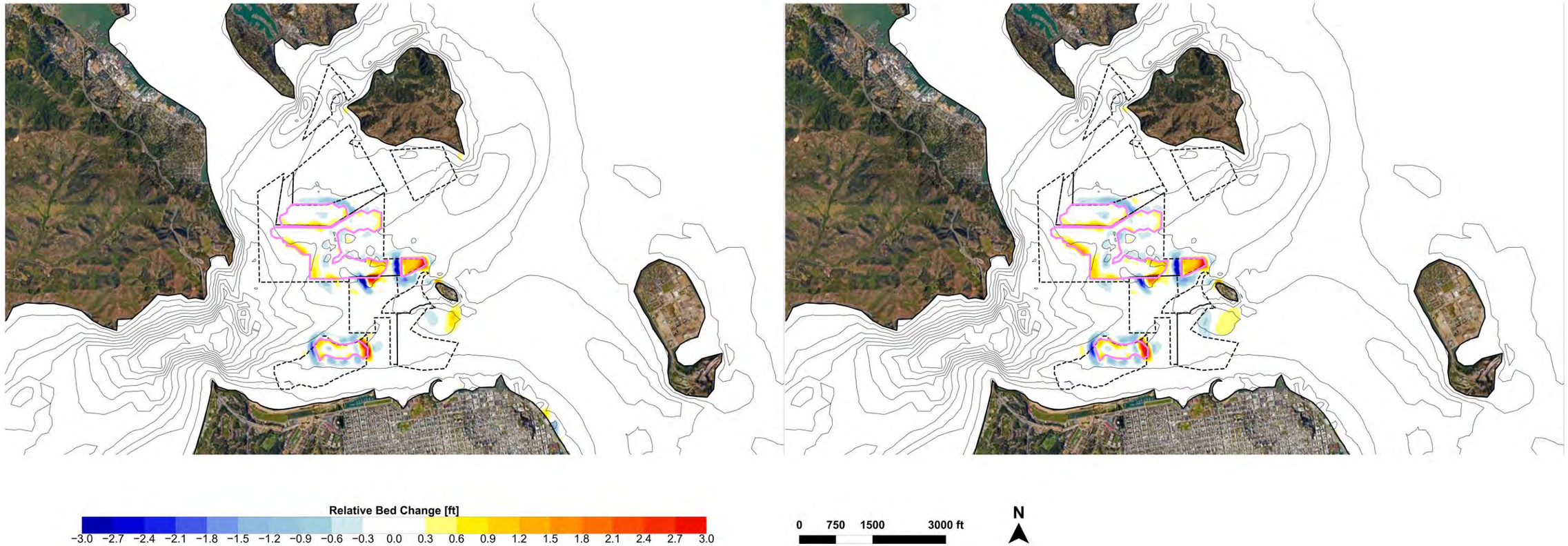

Notes:

1. Relative Bed Change was calculated by subtracting bed changes predicted for Proposed Mining from bed changes predicted for No Proposed Mining.
2. Fully Dynamic Coupling Approach indicates continual calculation of bed change at each hydrodynamic model time step that results in continual changes in hydrodynamics.
3. Decoupled Approach indicates that hydrodynamics are not affected by ongoing bed changes, resulting in greater overall predicted Relative Bed Change due to Proposed Mining (conservative assumption).
4. Magenta polygons represent the mining areas that were deepened within the lease areas.

Figure 5.1:

4-Month Bed Change Differences Caused by Proposed Mining Relative to No Proposed Mining for Decoupled Approach Between Hydrodynamics and Morphology (Left) and Fully Dynamic Coupling Approach (Right) During Low-Flow Simulation, Central Bay

COAST & HARBOR ENGINEERING

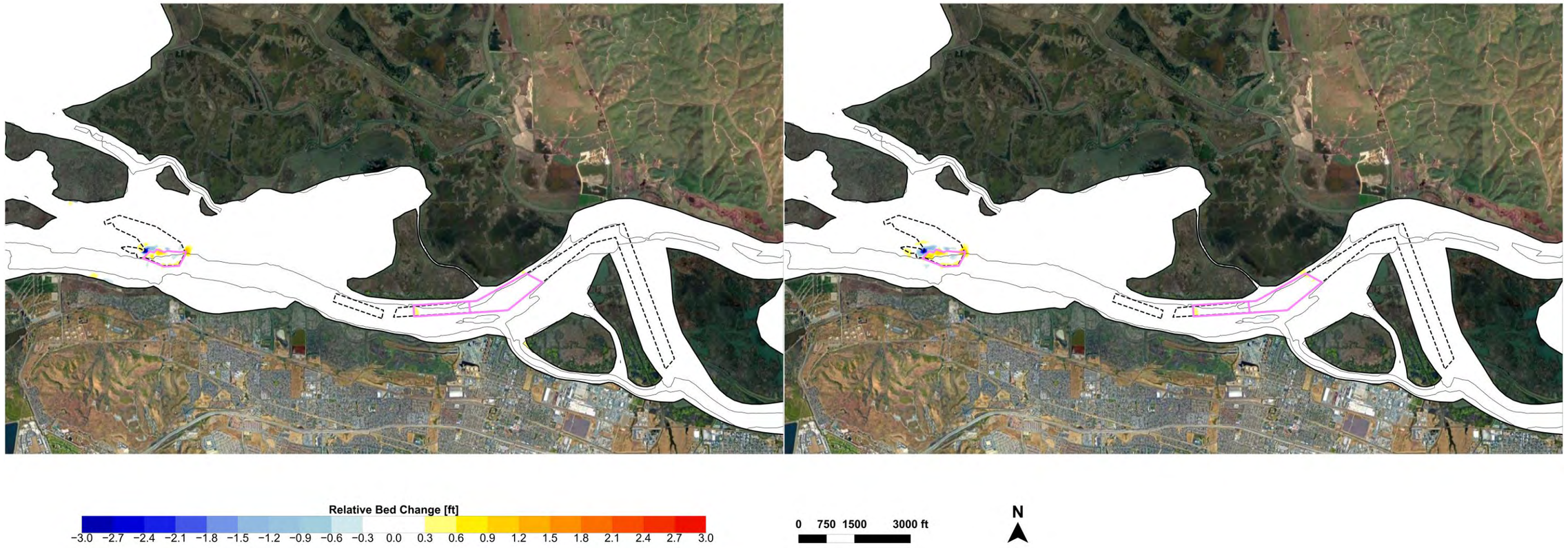

Notes:

1. Relative Bed Change was calculated by subtracting bed changes predicted for Proposed Mining from bed changes predicted for No Proposed Mining.
2. Fully Dynamic Coupling Approach indicates continual calculation of bed change at each hydrodynamic model time step that results in continual changes in hydrodynamics.
3. Decoupled Approach indicates that hydrodynamics are not affected by ongoing bed changes, resulting in greater overall predicted Relative Bed Change due to Proposed Mining (conservative assumption).
4. Magenta polygons represent the mining areas that were deepened within the lease areas.

Figure 5.2:

4-Month Bed Change Differences Caused by Proposed Mining Relative to No Proposed Mining for Decoupled Approach Between Hydrodynamics and Morphology (Left) and Fully Dynamic Coupling Approach (Right) During Low-Flow Simulation, Suisun Bay

COAST & HARBOR ENGINEERING

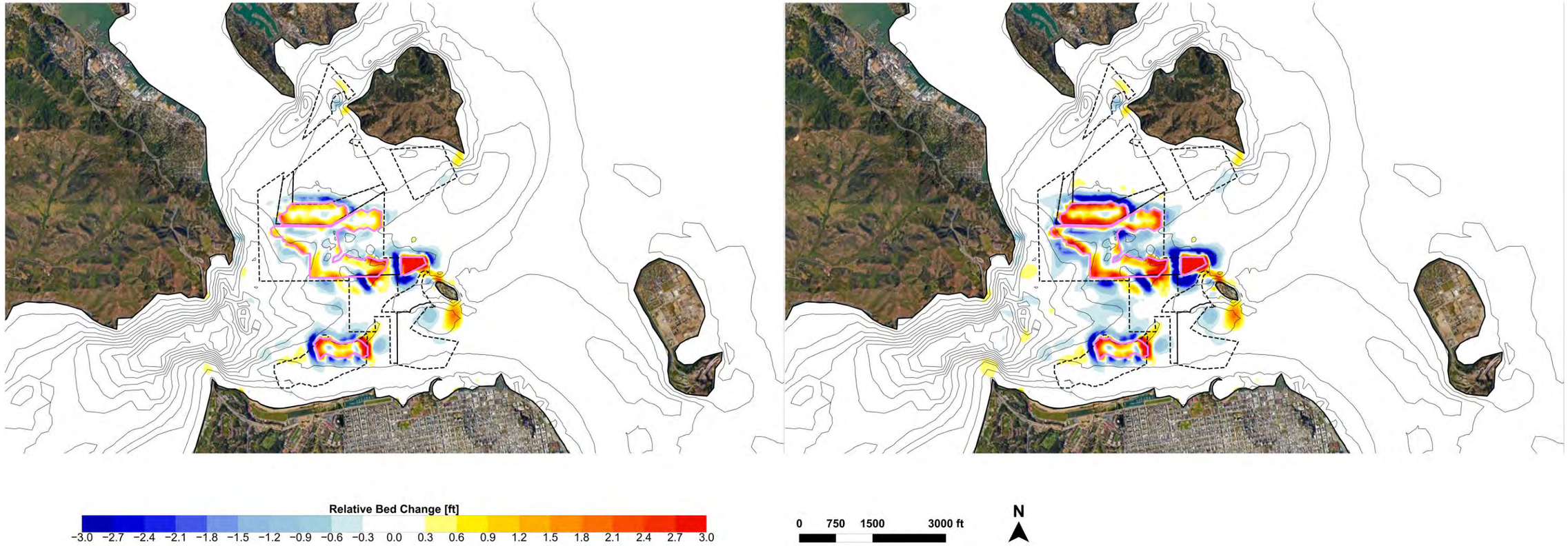

Notes:

1. Relative Bed Change was calculated by subtracting bed changes predicted for Proposed Mining from bed changes predicted for No Proposed Mining.
2. Both simulations shown above were performed using the multi-fraction modeling approach; however, the left panel shows results for the variable grain size distribution based on measurements, and the right panel shows results when all 8 sand fractions are set to a constant size of 0.25mm.
3. Magenta polygons represent the mining areas that were deepened within the lease areas.

Figure 5.3:

One-Year Bed Change Differences Caused by Proposed Mining Relative to No Proposed Mining for Variable Grain Sizes (Left) and 0.25mm Sand Median Grain Size Domain-Wide (Right) During High-Flow Simulation, Central Bay

COAST & HARBOR ENGINEERING

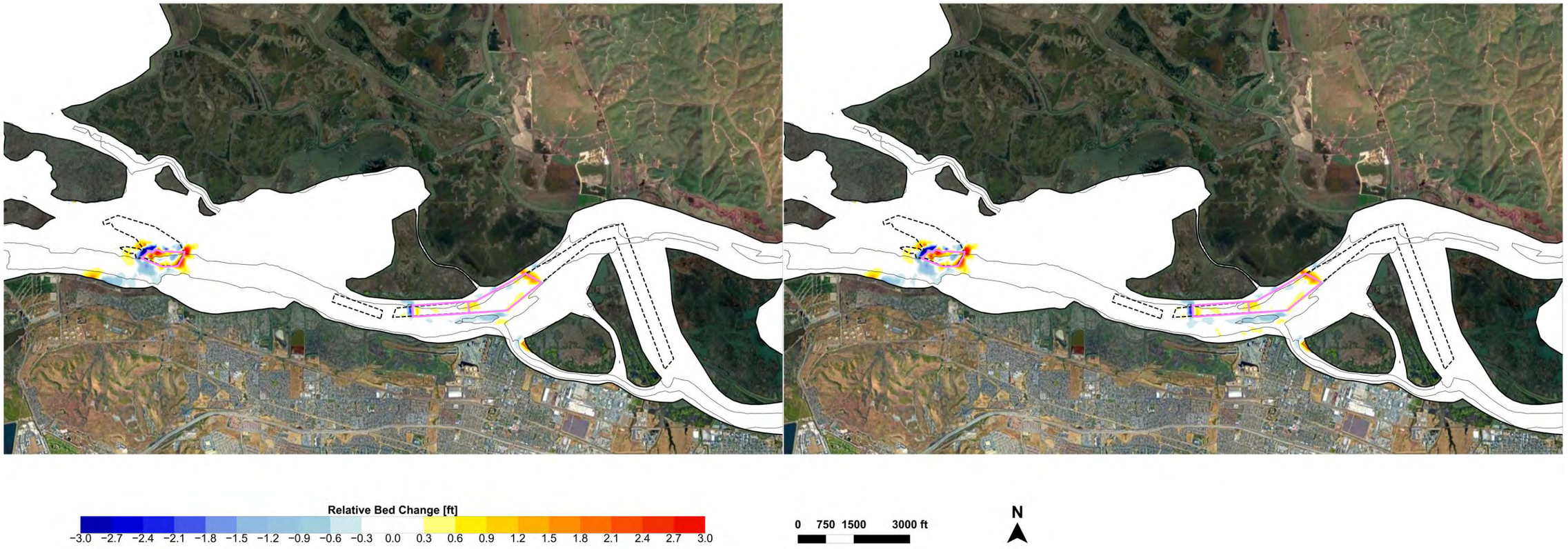

Notes:

1. Relative Bed Change was calculated by subtracting bed changes predicted for Proposed Mining from bed changes predicted for No Proposed Mining.
1. Both simulations shown above were performed using the multi-fraction modeling approach; however, the left panel shows results for the variable grain size distribution based on measurements, and the right panel shows results when all 8 sand fractions are set to a constant size of 0.25mm.
2. Magenta polygons represent the mining areas that were deepened within the lease areas.

Figure 5.4:

One-Year Bed Change Differences Caused by Proposed Mining Relative to No Proposed Mining for Variable Grain Sizes (Left) and 0.25mm Sand Median Grain Size Domain-Wide (Right) During High-Flow Simulation, Suisun Bay

COAST & HARBOR ENGINEERING

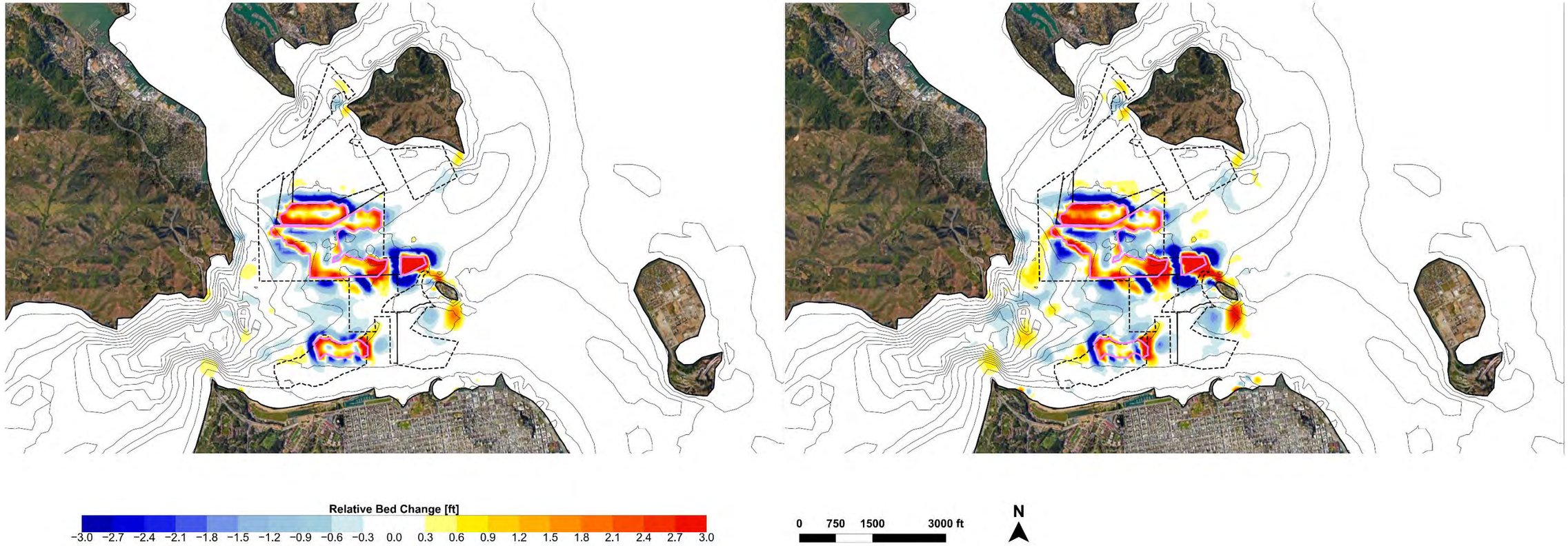

Notes:

1. Relative Bed Change was calculated by subtracting bed changes predicted for Proposed Mining from bed changes predicted for No Proposed Mining.
2. Both simulations shown above were performed using the entire domain set to constant median sand grain size of 0.25mm; similarities in potential impacts between the left and right panels indicates that choice of sand transport formulation (multi-fraction formulation at left, Van Rijn formulation at right) has minimal influence on the impact analysis results.
3. Magenta polygons represent the mining areas that were deepened within the lease areas.

Figure 5.5:

One-Year Bed Change Differences Caused by Proposed Mining Relative to No Proposed Mining for Multi-Fraction Transport Formulation (Left) and van Rijn Transport Formulation (Right) with 0.25mm Sand Grain Size Domain-Wide, During High-Flow Simulation, Central Bay

COAST & HARBOR ENGINEERING

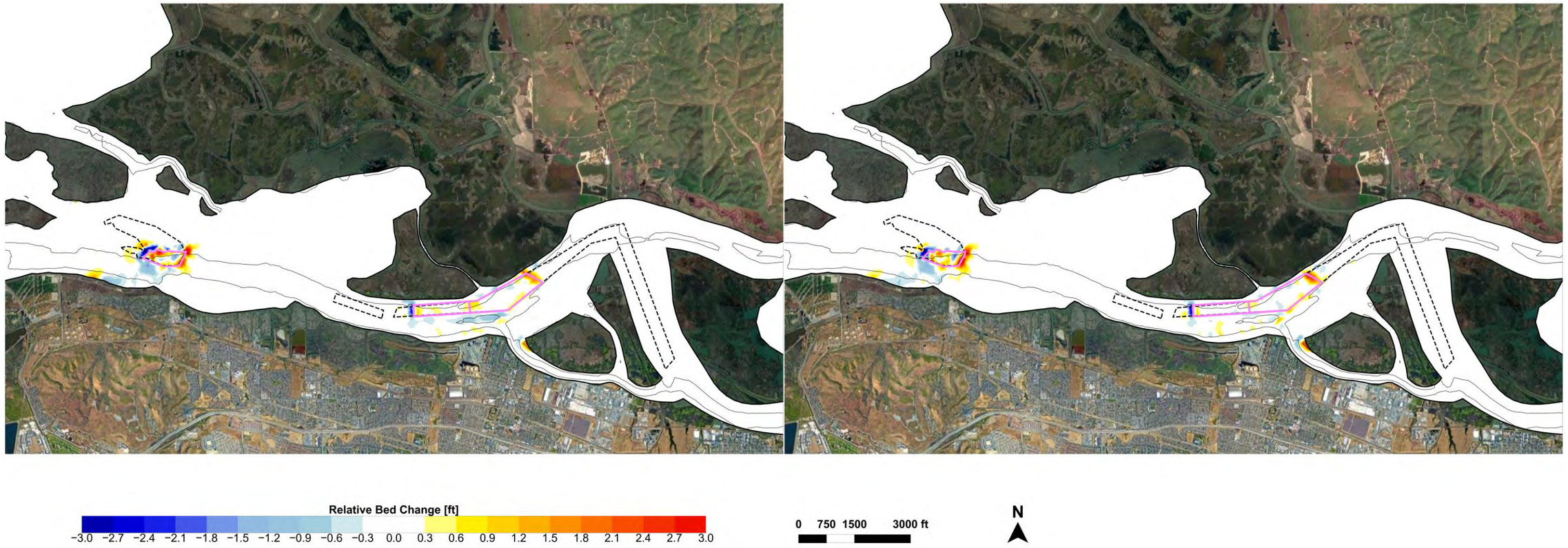

Notes:

1. Relative Bed Change was calculated by subtracting bed changes predicted for Proposed Mining from bed changes predicted for No Proposed Mining.
2. Both simulations shown above were performed using the entire domain set to constant median sand grain size of 0.25mm; similarities in potential impacts between the left and right panels indicates that choice of sand transport formulation (multi-fraction formulation at left, Van Rijn formulation at right) has minimal influence on the impact analysis results.
3. Magenta polygons represent the mining areas that were deepened within the lease areas.

Figure 5.6:

One-Year Bed Change Differences Caused by Proposed Mining Relative to No Proposed Mining for Multi-Fraction Transport Formulation (Left) and van Rijn Transport Formulation (Right) with 0.25mm Sand Grain Size Domain-Wide, During High-Flow Simulation, Suisun Bay

COAST & HARBOR ENGINEERING